



Molecular Crystals and Liquid Crystals

Publication details, including instructions for authors and
subscription information:

<http://www.tandfonline.com/loi/gmcl18>

The Effect of Electric Fields on Blue Phases

H. S. Kitzerow^a

^a Iwan-N.-Stranski-Institut, Sekr. ER 11, Technische Universität
Berlin, Str. des 17. Juni 135, 1000, Berlin, 12, FRG
Version of record first published: 24 Sep 2006.

To cite this article: H. S. Kitzerow (1991): The Effect of Electric Fields on Blue Phases, *Molecular Crystals and Liquid Crystals*, 202:1, 51-83

To link to this article: <http://dx.doi.org/10.1080/00268949108035659>

PLEASE SCROLL DOWN FOR ARTICLE

Full terms and conditions of use: <http://www.tandfonline.com/page/terms-and-conditions>

This article may be used for research, teaching, and private study purposes. Any substantial or systematic reproduction, redistribution, reselling, loan, sub-licensing, systematic supply, or distribution in any form to anyone is expressly forbidden.

The publisher does not give any warranty express or implied or make any representation that the contents will be complete or accurate or up to date. The accuracy of any instructions, formulae, and drug doses should be independently verified with primary sources. The publisher shall not be liable for any loss, actions, claims, proceedings, demand, or costs or damages whatsoever or howsoever caused arising directly or indirectly in connection with or arising out of the use of this material.

The Effect of Electric Fields on Blue Phases

H.-S. KITZEROW

Iwan-N.-Stranski-Institut, Sekr. ER 11, Technische Universität Berlin, Str. des 17. Juni 135, 1000 Berlin 12, FRG

(Received July 28, 1990)

An experimental review on electric field effects in blue phases is presented. Electric fields have a profound effect on these phases which appear in chiral liquid crystals. In addition to producing electrostrictive effects on blue phase lattices, they also cause new field induced phases—tetragonal BPX, hexagonal BPH^{3D} and BPH^{2D}, and possible other phases yet to be identified. In recent experiments on BPIII for materials with negative dielectric anisotropy, it was found that electric fields cause a dramatic increase in the otherwise weak BPIII selective reflection. These experimental results were discussed with respect to possible models for the unknown structure of BPIII. Recently, efforts were also made to investigate the dynamics of different electrooptic effects more precisely.

Keywords: liquid crystals, electro-optical effects, electrostriction, blue phases, field-induced phase transition

I. INTRODUCTION

The blue phases of chiral liquid crystals were first observed more than hundred years ago¹ but studied extensively only during the past two decades.^{2–6} Although these phases occur very close to the clearing temperature, between either a cholesteric^{7–9} or smectic phase¹⁰ and the isotropic liquid, many of their properties exhibit a formal analogy to solid crystals. The most striking of these properties are Bragg reflection in the visible wavelength range indicating a spatially periodic structure with lattice constants of several hundred nm^{11,12} and the occurrence of liquid single crystals,^{13–19} i.e. liquid crystal droplets in an isotropic environment which exhibit no spherical shape but facets similar to solid crystals.

At zero field, three modifications BPI, BPII and BPIII (the latter also called 'blue fog')¹⁴ have yet been observed.^{2–6,20–22} Their numbers indicate the sequence of occurrence with increasing temperature^{23–24} and correspond also to the sequence of their occurrence with increasing chirality in chiral racemic phase diagrams.^{25,26} Both calorimetric^{23,27–30} and dilatometric³¹ measurements indicate that the transitions between each of these phases are of first order, but the latent heats for the phase transitions from the cholesteric to a blue phase and from a special blue phase to another blue phase modification are very small (≈ 2 – 18 J/mole for cholesteryl-nonanoate²⁸) compared to the transition enthalpy at the clearing point (≈ 170 J/mole for cholesteryl-nonanoate).²⁸

A. Saupe⁸ proposed a director field with chiral cubic symmetry for blue phases. In terms of an order parameter, such structures can be described by the anisotropic part ε_{ij} of the dielectric tensor, given in general by the Fourier series³²⁻³⁴

$$\varepsilon_{ij}(r) = \sum_h \sum_k \sum_l \frac{1}{\sqrt{N}} \tilde{\varepsilon}_{ij}(q) e^{iq \cdot r} \quad (1)$$

where N is the multiplicity of equivalent families of planes (hkl), and q are the respective reciprocal lattice vectors. For each q , the tensor coefficient $\tilde{\varepsilon}(q)$ exhibits the general form

$$\begin{aligned} \tilde{\varepsilon}(q) = \frac{1}{2} \left\{ \varepsilon_2 e^{i\psi_2} \begin{pmatrix} 1 & i & 0 \\ i & -1 & 0 \\ 0 & 0 & 0 \end{pmatrix} + \varepsilon_1 e^{i\psi_1} \begin{pmatrix} 0 & 0 & 1 \\ 0 & 0 & i \\ 1 & i & 0 \end{pmatrix} + \sqrt{\frac{2}{3}} \varepsilon_0 e^{i\psi_0} \begin{pmatrix} -1 & 0 & 0 \\ 0 & -1 & 0 \\ 0 & 0 & 2 \end{pmatrix} \right. \\ \left. + \varepsilon_{-1} e^{i\psi_{-1}} \begin{pmatrix} 0 & 0 & -1 \\ 0 & 0 & i \\ -1 & i & 0 \end{pmatrix} + \varepsilon_{-2} e^{i\psi_{-2}} \begin{pmatrix} 1 & -i & 0 \\ -i & -1 & 0 \\ 0 & 0 & 0 \end{pmatrix} \right\}, \quad (2) \end{aligned}$$

where ε_0 , $\varepsilon_{\pm 1}$, and $\varepsilon_{\pm 2}$ are the amplitudes of five different modes (since ε_{ij} is symmetric and traceless and thus exhibits five independent components). The optical selection rules for these chiral cubic structures were derived by R. M. Hornreich and S. Shtrikman³³ and for hexagonal structures by B. Jérôme and P. Pieranski.³⁵ According to these selection rules BPI exhibits a body centered cubic structure (Figure 1) described by the space group $I 4_1 32 (O^8)$ and BPII exhibits a simple cubic structure $P 4_2 32 (O^2)$.³⁶⁻⁴⁰ According to the defect theory by Meiboom *et al.*,^{41,42} these structures can be also considered as a regular lattice of disclinations, or a lattice of double twist cylinders (Figure 2).^{43,44} The modification BPIII exhibit a broad selective reflection band with very low intensity.^{45,46} Its structure is yet unknown.

The following experimental techniques were used to obtain informations on blue phase structures from their Bragg reflection:

- (i) Spectroscopic measurement of the Bragg wavelengths at normal incidence^{11,12,15} \rightarrow ratios of the interplanar distances
- (ii) Microscopic observation of the rotational symmetry of single crystals¹⁴⁻¹⁸ \rightarrow correspondence of the observed peaks to ($h00$), ($hh0$) or (hhh) planes,
- (iii) Investigation of the angular dependence of the selective reflection⁴⁷⁻⁴⁹ \rightarrow multiplicity of equivalent planes,
- (iv) Measurement of the Mueller matrix at non-normal incidence⁵⁰⁻⁵² \rightarrow amplitudes ε_m of the modes for the corresponding reciprocal lattice vector,^{33,53}
- (v) Observation of single crystals illuminated with white light in back reflection using a rotating microscope stage^{38,39,54} (Figure 3a) \rightarrow interplanar angles and interplanar distances,
- (vi) Kossel diagrams (conoscopic observation of single crystals using monochromatic light, Figure 3b,c)⁵⁵ \rightarrow interplanar angles and interplanar distances.

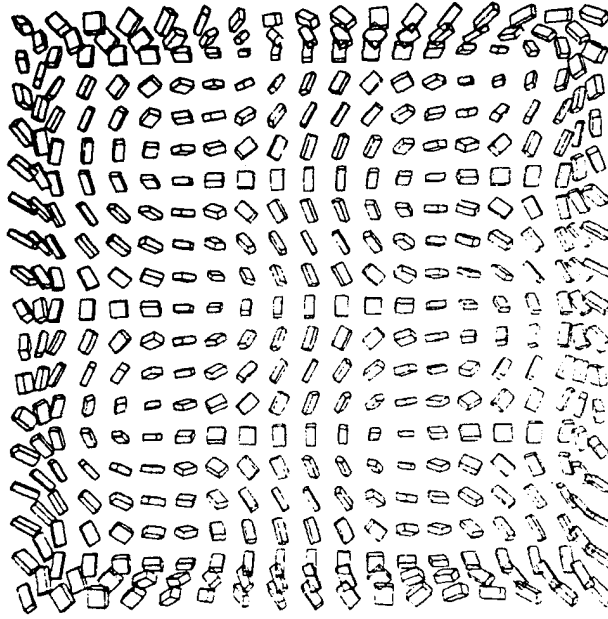


FIGURE 1 Model for BPI: Visualization of the tensor order parameter along the planes of type (100) in a bcc unit cell with $I 4_1 32 (O^*)$ symmetry. The edges of the quaders represent the direction of the eigenvectors and the eigenvalues of the dielectric tensor (From P. Pieranski, R. Barbet-Massin and P. E. Cladis¹⁸).

The latter method, developed by P. E. Cladis, T. Garel and P. Pieranski,⁵⁵ has been proved to be very powerful. According to the Bragg condition

$$\lambda_{hkl} = 2 \cdot \bar{n} \cdot d_{hkl} \cdot \cos \vartheta \quad (3)$$

or (in the reciprocal space)

$$q = k - k'$$

Kossel cones⁵⁶ with an aperture angle

$$\vartheta = \arccos \frac{\lambda_{hkl}}{2 \cdot \bar{n} \cdot d_{hkl}} = \arccos \frac{|q_{hkl}|}{2 |k|} \quad (4)$$

occur when single crystals are illuminated with convergent monochromatic radiation. For blue phases, cone sections of these cones can be observed optically in the focal plane of a microscope lens. Each of these Kossel lines represents the orientation and the interplanar distance of a family of planes in the lattice (Figure 3b, c).

Informations on the space groups of BPI and BPII were also obtained from the growth rates observed for the facets of single crystals. The single crystals of BPII

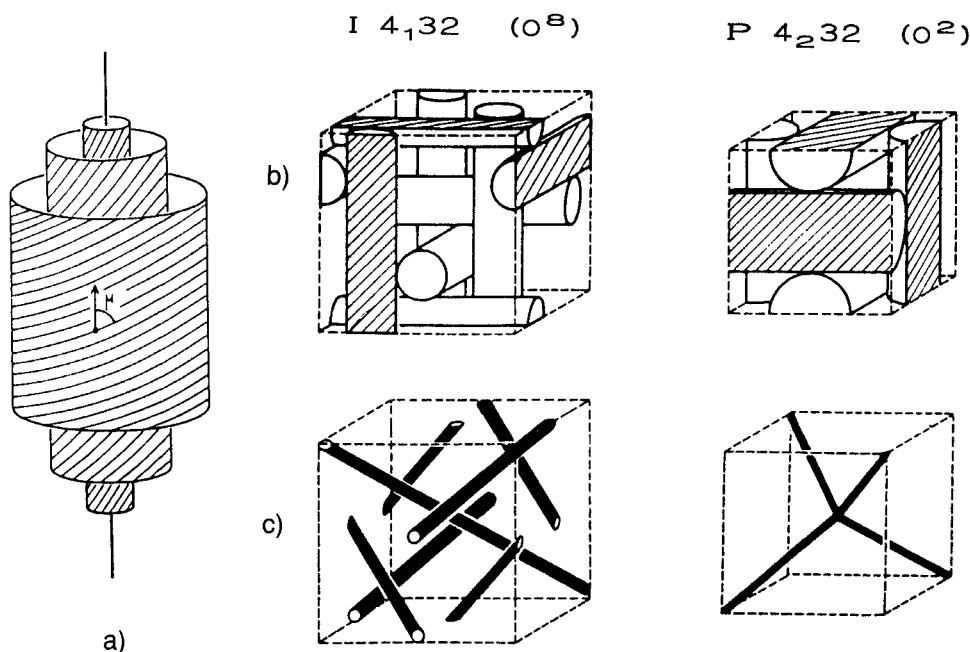


FIGURE 2 a) Director field in a double twist cylinder. b) Configuration of double twist cylinders for the space groups $I 4_1 32 (O^8)$ of BPI and $P 4_2 32 (O^2)$ of BPIL. c) Disclination tubes occurring in the respective unit cells according to the model from S. Meiboom *et al.*^{41,42} (Figures from E. Dubois-Violette and B. Pansu⁴⁴).

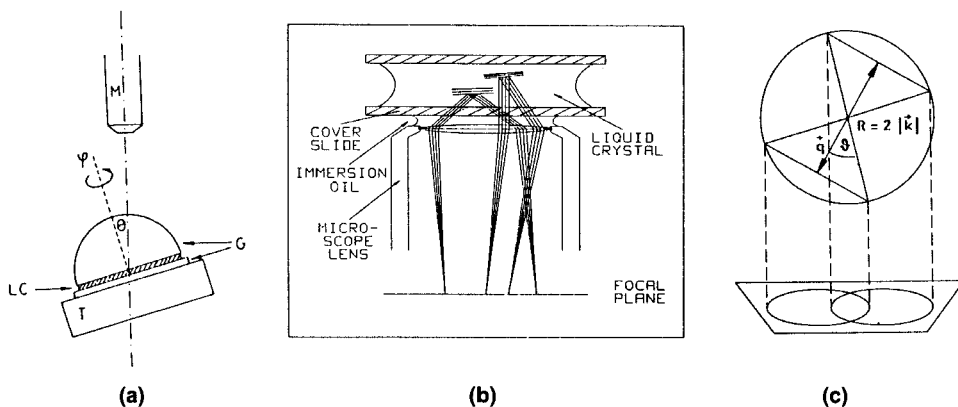


FIGURE 3 Optical methods used to investigate the structure of blue phases: a) Observation of single crystals in reflection using a polarizing microscope equipped with a rotating hot stage to determine the interplanar angles. (From W. Kuczyński³⁸). b) Experimental setup for the observation of Kossel diagrams occurring if single crystals are illuminated with convergent, monochromatic light. A family of planes is represented by an elliptical Kossel ring being a cone section of the Kossel cone perpendicular to the planes. c) Construction of Kossel diagrams in the reciprocal space by means of a sphere twice as large as the Ewald sphere. Each Kossel line is given by a planar projection of the intersection line between the respective Kossel cone and the surface of this sphere.

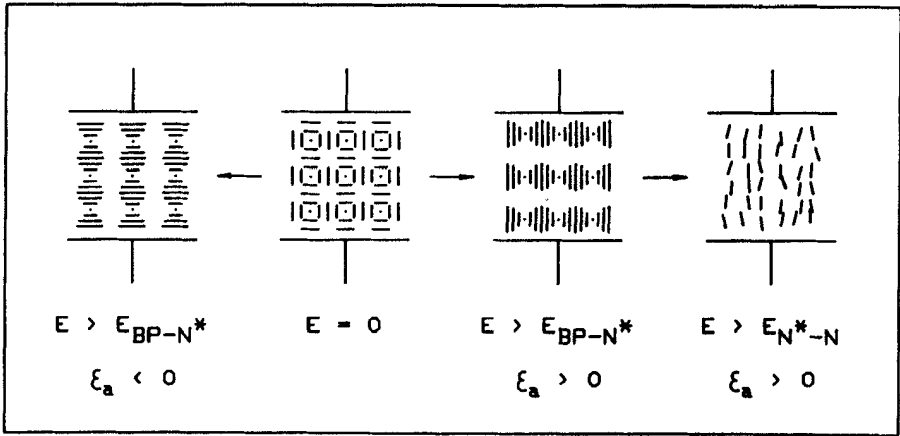
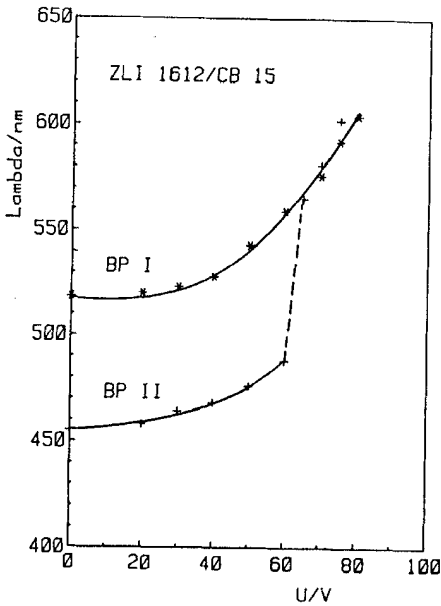
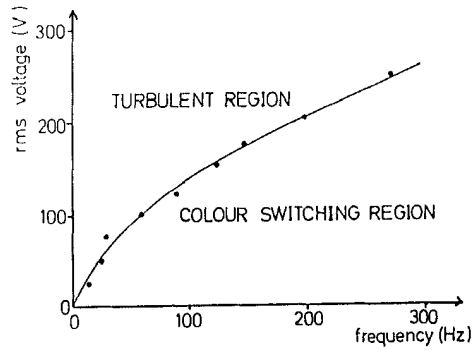


FIGURE 4 Schematic representation of the field-induced phase transitions from blue phases to the cholesteric phase (with different orientations depending on the sign of ϵ_a) and to the homeotropic nematic state (only for $\epsilon_a > 0$).



(a)



(b)

FIGURE 5 a) Dependence of the selective reflection bands on the applied electric field strength (rms, frequency = 1 kHz) for BPI (110) at $t = 22.3^\circ\text{C}$ and for BPII (100) at $t = 23.4^\circ\text{C}$ in a mixture with positive dielectric anisotropy (59.7% CB15, 40.3% ZLI 1612). (From G. Heppke *et al.*⁶²). b) Dependence of the onset of turbulence in BPII on applied voltage (sample thickness = 23 μm) and frequency for a mixture with positive dielectric anisotropy (from H. Gleeson *et al.*⁶³).

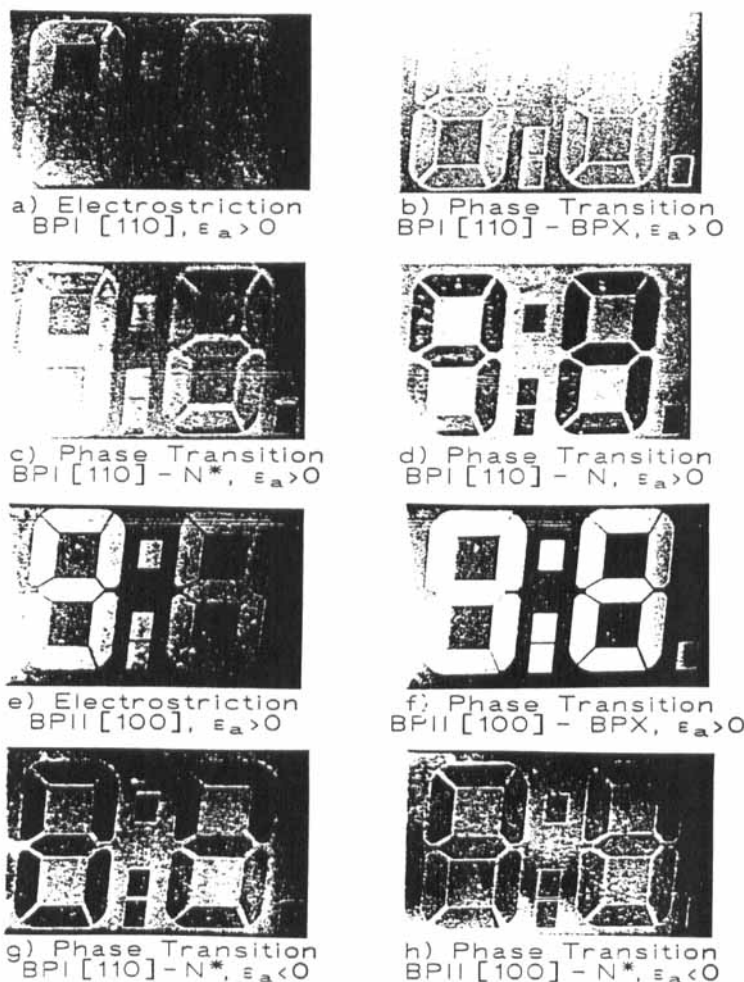


FIGURE 6 Electrooptic effects on blue phases, observed in $14\ \mu\text{m}$ cells with TN type surface treatment under the influence of ac voltages up to 80 V.

are usually limited by (110) facets⁵⁷ and exhibit a quadratic shape for observation along one of their fourfold axes.^{14,15} Very rich faceted three dimensional crystals for BPI were described by P. Pieranski *et al.*¹⁶⁻¹⁸ and by H. Stegemeyer *et al.*^{4,19} The sequence of facets observed for BPI with increasing growth rate are (110), (211), (310), (111), (321).¹⁸ This sequence is in agreement with the Donnay-Harker-rule⁵⁸ for the space group $I4_132$ (O^8).⁵⁹

Much experimental work during the last decade was devoted to field effects since the first observations of electrooptical effects in blue phases. Between 1980 and 1982, D. Armitage and R. J. Cox⁶⁰ reported on a field-induced phase transition from blue phases to the cholesteric phase (Figure 4), P. L. Finn and P. E. Cladis⁶¹ observed hydrodynamic instabilities under the influence of an electric field (dc or ac), and G. Heppke, M. Krumrey and F. Oestreicher⁶² found a wavelength shift

TABLE I

Blue phase systems investigated under the influence of an electric field (a,b) and the chemical structure of their components (c,d)

a) Materials with positive dielectric anisotropy.

| System: | References: |
|-------------------------------------|--|
| BOBC / CHCP | <119> |
| CB15 / E9 | <57>, <87>, <88>, <93>, <80>, <35>, <68>, <89> |
| CB15 / M18 | <61>, <73>, <90>, <84>, <80> |
| CB15 / M24 | <90> |
| CB15 / RO-TN404 | <62>, <76>, <84> |
| CB15 / ZLI1612 | <62>, <84> |
| CB15 / ZLI1840 | <83>, <57> |
| CB15 / ZLI1841 | <83> |
| CB15 / CE1 / CE2 / CE3 / E9 / K18 | <120> |
| CBMBB | <83> |
| CBMBB / CPMBB | <83> |
| CE1 / CE2 / CE3 / E7 / E49 / K18 | <120> |
| CE1 / CE2 / K18 | <91> |
| CE1 / CE2 / CE3 / E310 | <120>, <121> |
| CE1 / CE2 / CE3 / PG296 | <121> |
| CE2 / ZLI1083 / RO 3478 | <89> |
| CC / CL | <103> |
| CP / 2-7A0B | <61> |
| CP / CB00A | <61> |
| CP / M24 | <61> |
| MHCS | <60> |
| PBBN / RO-TN404 | <100> |
| S811 / N5 | <69> |
| TM74A / TM74B / TM75A / TM75B / E49 | <63> |

b) Materials with negative dielectric anisotropy.

| | |
|-------------------|--------------------------------------|
| CE2 | <60> |
| CE2 / CE3 / CCN55 | <113> |
| CE2 / ZLI1014 | <61> |
| CM / CCN55 | <104> |
| CP / ZLI1014 | <61> |
| MBBOCB / ZLI2585 | <94>, <67> |
| S811 / EN18 | <66>, <76>, <94>, <67>, <114>, <115> |

c) Chemical Structure of the chiral compounds used in these systems.

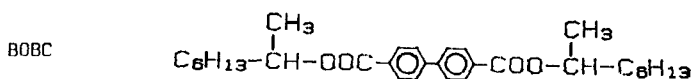
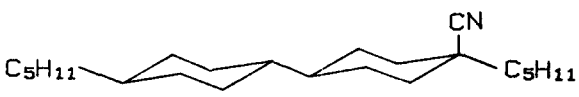


TABLE I (continued)

| | |
|----------------|--|
| CB15 (BDH) | $\text{CH}_3-\text{CH}_2-\overset{\text{CH}_3}{\underset{ }{\text{CH}}}-\text{CH}_2-\text{C}_6\text{H}_4-\text{C}_6\text{H}_4-\text{CN}$ |
| CBMBB | $\text{CH}_3-\text{CH}_2-\overset{\text{CH}_3}{\underset{ }{\text{CH}}}-\text{CH}_2-\text{C}_6\text{H}_4-\text{COO}-\text{C}_6\text{H}_4-\text{C}_6\text{H}_4-\text{CN}$ |
| CC, CM, CL, CP | $\text{R}-\text{Cyclohexane}-\text{CH}(\text{CH}_3)-(\text{CH}_2)_3-\text{CH}(\text{CH}_3)_2$ <p style="text-align: right;"> $\text{R} = \text{C1}$ $\text{CH}_3-(\text{CH}_2)_{12}-\text{COO}$ $\text{CH}_3-(\text{CH}_2)_{10}-\text{COO}$ $\text{CH}_3-\text{CH}_2-\text{COO}$ </p> |
| CE1 (BDH) | $\text{CH}_3-\text{CH}_2-\overset{\text{CH}_3}{\underset{ }{\text{CH}}}-\text{CH}_2-\text{C}_6\text{H}_4-\text{C}_6\text{H}_4-\text{COO}-\text{C}_6\text{H}_4-\text{CN}$ |
| CE2 (BDH) | $\text{CH}_3-\text{CH}_2-\overset{\text{CH}_3}{\underset{ }{\text{CH}}}-\text{CH}_2-\text{C}_6\text{H}_4-\text{C}_6\text{H}_4-\text{COO}-\text{C}_6\text{H}_4-\text{CH}_2-\overset{\text{CH}_3}{\underset{ }{\text{CH}}}-\text{CH}_2-\text{CH}_3$ |
| CE3 (BDH) | $\text{CH}_3-\text{CH}_2-\overset{\text{CH}_3}{\underset{ }{\text{CH}}}-\text{CH}_2-\text{C}_6\text{H}_4-\text{C}_6\text{H}_4-\text{COO}-\text{C}_6\text{H}_4-\text{OC}_6\text{H}_{13}$ |
| CPMBB | $\text{CH}_3-\text{CH}_2-\overset{\text{CH}_3}{\underset{ }{\text{CH}}}-\text{CH}_2-\text{C}_6\text{H}_4-\text{COO}-\text{C}_6\text{H}_4-\text{CN}$ |
| MHCS | $\text{C}_2\text{H}_5-\overset{\text{CH}_3}{\underset{ }{\text{CH}}}-(\text{CH}_2)_3-\text{C}_6\text{H}_4-\text{CH}=\text{CH}-\text{C}_6\text{H}_4-\text{CN}$ |
| MBBOCB | $\text{CH}_3-\text{CH}_2-\overset{\text{CH}_3}{\underset{ }{\text{CH}}}-\text{CH}_2-\text{C}_6\text{H}_4-\text{COO}-\overset{\text{Cl}}{\text{C}_6\text{H}_3}-\text{OOC}-\text{C}_6\text{H}_4-\text{CH}_2-\overset{\text{CH}_3}{\underset{ }{\text{CH}}}-\text{CH}_2-\text{CH}_3$ |
| PBBN | $\text{C}_6\text{H}_5-\text{OOC}-\text{C}_6\text{H}_4-\text{C}_6\text{H}_4-\text{C}_5\text{H}_{11}$ $\text{C}_6\text{H}_5-\text{OOC}-\text{C}_6\text{H}_4-\text{C}_6\text{H}_4-\text{C}_5\text{H}_{11}$ |

TABLE I (continued)

| | |
|---|--|
| S811 (Merck) | $\text{C}_6\text{H}_{13}-\text{O}-\text{C}_6\text{H}_4-\text{COO}-\text{C}_6\text{H}_4-\text{COO}-\overset{\text{CH}_3}{\underset{ }{\text{CH}}}-\text{C}_6\text{H}_{13}$ |
| TM74A, TM74B, TM75A and TM75B are cholesteric thermochromic mixtures from British Drug House (BDH). | |
| d) Chemical Structure of the non-chiral compounds used in these systems. | |
| 2-7A0B | $\text{C}_7\text{H}_{15}-\text{O}-\text{C}_6\text{H}_4-\text{N}(\text{O})=\text{N}-\text{C}_6\text{H}_4-\text{O}-\text{C}_7\text{H}_{15}$ |
| CB00A | $\text{C}_6\text{H}_{17}-\text{O}-\text{C}_6\text{H}_4-\text{CH}=\text{N}-\text{C}_6\text{H}_4-\text{CN}$ |
| CCN55 (Merck) |  |
| CHCP | $\text{C}_m\text{H}_{2m+1}-\text{C}_6\text{H}_4-\text{COO}-\text{C}_n\text{H}_{2n+1}$ (m,n) = (3,2);(4,2);(5,1);(4,4) |
| K18,M18,M24 (BDH) | $\text{R}-\text{C}_6\text{H}_4-\text{C}_6\text{H}_4-\text{CN}$ R = C ₆ H ₁₃ - C ₆ H ₁₃ -O- C ₆ H ₁₇ -O- |
| N5 (Merck) | $\text{CH}_3-\text{O}-\text{C}_6\text{H}_4-\text{N}(\text{O})=\text{N}-\text{C}_6\text{H}_4-\text{R}$ R = -C ₂ H ₅ -C ₄ H ₉ |
| PG296 | $\text{CH}_3-\text{Si}-\text{O}-\left[\overset{\text{CH}_3}{\underset{ }{\text{Si}}}-\text{O} \right]_n-\left[\overset{\text{CH}_3}{\underset{ }{\text{Si}}}-\text{O} \right]_m-\text{Si}-\text{O}-\text{CH}_3$ (CH ₂) ₆ -O-C ₆ H ₄ -C ₆ H ₄ -CN (CH ₂) ₄ -O-C ₆ H ₄ -COO-C ₆ H ₄ -C ₉ H ₇ m = n = 25 |
| ZLI1014 (Merck) | $\text{C}_5\text{H}_{11}-\text{C}_6\text{H}_4-\text{C}_6\text{H}_4-\text{COO}-\overset{\text{CN}}{\text{C}_6\text{H}_4}-\text{C}_7\text{H}_{15}$ |

The other abbreviations used in Table I correspond to wide temperature range nematic mixtures produced by the companies British Drug House (E7, E9, E49, E310), Chisso (EN18), Hoffmann La Roche (RO-3487) and Merck (ZLI1083, ZLI1612, ZLI1840, ZLI1841, ZLI2585), respectively.

of the Bragg peaks by applying ac voltages (Figures 5, 6). More detailed studies show that hydrodynamic instabilities can be avoided by using high frequencies (Figure 5b).⁶³

The materials used to study electric field effects are either polar chiral compounds or solutions of a chiral dopant in a nematic solvent consisting of polar molecules (Table I). A crucial parameter for the electric field effects is the dielectric anisotropy $\epsilon_a = \epsilon_{\parallel} - \epsilon_{\perp}$, where ϵ_{\parallel} and ϵ_{\perp} are the values of the dielectric constant for a field applied parallel and perpendicular to the director, respectively. To characterize blue phase mixtures, these values can be measured in the nematic phase of the respective racemic mixture close to the clearing temperature. The sign of ϵ_a depends on the angle between the permanent dipole moment of a molecule and the molecular long axis.⁶⁴

Several general review articles on blue phases from both the experimental²⁻⁴ and the theoretical point of view^{5,6} were published during the last few years. An extended reference list with 247 references about blue phases was given in Reference 65. The aim of this review article is to focus on the behaviour of blue phases under the influence of an electric field and to give a summary of the experimental results obtained yet. In the following section, the field effects on the cubic structures BPI and BP II are described, which correspond to continuous deformations affecting both the lattice and the average molecular orientation, to reorientation of BP domains and to field-induced phase transitions. In section III recent observations on BP III and possible implications on the determination of this unknown structure are summarized. Section IV is devoted to recent results on the dynamics of the electrooptical effects. Finally, some open questions are mentioned in section V.

II. Influence of Electric Fields on BPI and BP II

1. Electrostriction

For weak electric fields, the continuous change of the Bragg wavelengths^{62,65-69} correspond to a continuous deformation of the cubic lattice. In the first experiments by G. Heppke *et al.*,⁶² the influence of an electric field on the (110)-peak in BPI and on the (100)-peak in BP II was investigated for mixtures with $\epsilon_a > 0$ (CB15/RO-TN404 and CB15/ZLI1612). In both cases, a red shift of the selective reflection was observed (Figure 6a,b,e), indicating an increase of the interplanar spacing along the field direction. However, a decrease of the Bragg wavelength was observed for the same selective reflection bands (the (110)-peak in BPI and the (100)-peak in BP II) when a mixture with $\epsilon_a < 0$ (S811/EN18) was investigated.⁶⁶ Moreover, the direction of the wavelength shift observed for BPI depends also on the orientation of the cubic lattice with respect to the field direction,^{66,67} an effect called anomalous electrostriction. Figure 7 shows the effects observed for BPI and BP II exhibiting two different orientations ($[001] \parallel E$ and $[011] \parallel E$), respectively, in both materials with positive (Figure 7a) and with negative dielectric anisotropy (Figure 7b).

Characteristic changes of the Kossel diagrams can be observed due to the continuous deformation of the blue phase structure.^{67,68} The Kossel diagrams of BPI

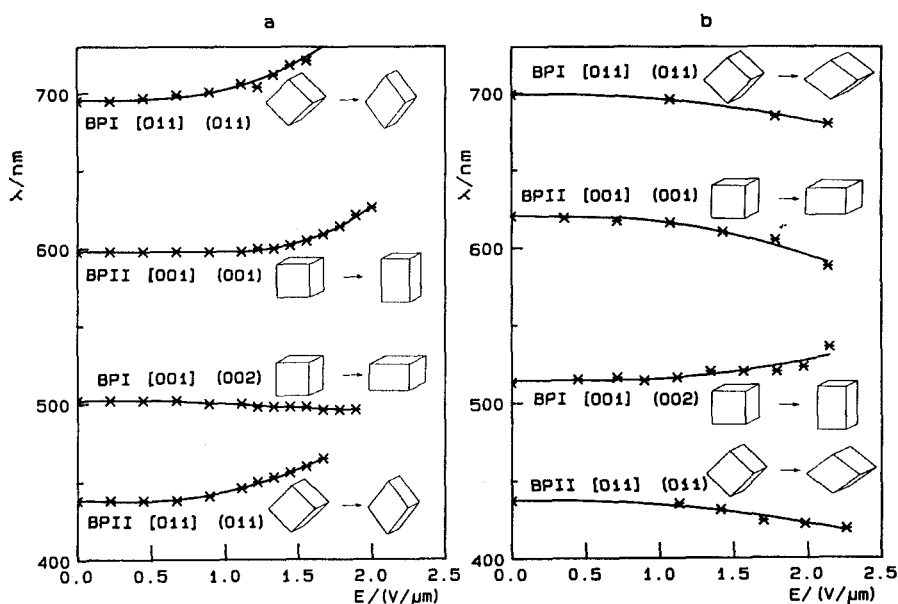


FIGURE 7 Bragg wavelengths corresponding to planes (hkl) versus applied field strength for BPI and BPII oriented with either a fourfold $[001]$ or with a twofold axis $[011]$ along the field direction. a) Spectroscopic values measured in back reflection for a mixture with *positive* dielectric anisotropy (49.2% CB15, 50.8% E9). (From G. Heppke *et al.*⁶⁸). b) Values determined by the Kossel method for a mixture with *negative* dielectric anisotropy (37.0% MW190, 63.0% ZLI 2585). (From G. Heppke *et al.*⁶⁷).

for observation along a fourfold axis $[001]$ (Figure 8, top) reveal a tetragonal structure under the influence of an electric field. The fourfold symmetry axis parallel to the field direction is preserved at non-zero field. However, the distance ξ_2 between the intersection points of the (101) and $(\bar{1}01)$ rings is larger than the diameter ξ_1 of the central (002) ring for systems with $\epsilon_a > 0$ whereas this distance ξ_2 is smaller than ξ_1 for systems with $\epsilon_a < 0$ at non-zero field strength. The construction of the respective reciprocal lattices (Figure 8, bottom) shows that for systems with positive dielectric anisotropy, the reciprocal lattice constant $2\pi/a_z$ along the field E is larger than the reciprocal lattice constants $2\pi/a_x$, $2\pi/a_y$, perpendicular to E .⁶⁸ A tetragonal structure deformed in the opposite direction is observed for systems with negative dielectric anisotropy.⁶⁷ Kossel diagrams of the deformed BPI and BPII structures were investigated also for other orientations.^{65,67,68}

Analogous to solid crystals,⁷⁰ the deformation of the lattice can be described by the (symmetric) strain tensor defined as

$$e_{ij} = \frac{1}{2} \left(\frac{\partial u_i}{\partial x_j} + \frac{\partial u_j}{\partial x_i} \right) \quad (5)$$

where x_1, x_2, x_3 are coordinates of a lattice point and u_1, u_2, u_3 are the components of the vector describing its displacement due to the deformation. The diagonal

FIGURE 8 Top: Kossel diagrams of the cubic BPI (center, top) and the continuously deformed BPI^d for observation along a fourfold axis [001]. Bottom: The respective reciprocal lattices in the (x, z) plane (construction as represented in Figure 3).

elements of the strain tensor correspond to principal strains while the off-diagonal elements correspond to shear strains. In order to describe the dependence of the strain on the electric field, the strain tensor can be expanded in powers of E :

$$e_{ij} = \sum_{k=1}^3 \gamma_{ijk} E_k + \sum_{k=1}^3 \sum_{l=1}^3 \gamma_{ijkl} E_k E_l + \dots \quad (6)$$

The linear term in this expansion, with the third rank piezoelectric tensor as its coefficient, vanishes since the deformation depend on the time average of the applied ac field. Thus, the lowest order term to describe the deformation of blue phase lattices in the electric field is the quadratic term which is connected to the strain tensor by the fourth rank electrostriction tensor.

V. E. Dmitrienko⁷¹ used the following expression for the free energy

$$F = F_o + \frac{1}{2} \Lambda_{iklm} u_{ik} u_{lm} - \frac{1}{16\pi} \chi_{iklm} E_i E_k E_l E_m - \frac{1}{8\pi} p_{iklm} E_i E_k u_{lm} \quad (7)$$

where Λ is the elasticity tensor, χ is the tensor of non-linear susceptibility and \mathbf{p} is the elasto-optic tensor. Summation over repeated indices is implied in Equation (7) as in (6). Minimization of the free energy with respect to the strain \mathbf{e} leads to a relation between the strain and the electric field E :

$$e_{ik} = \frac{1}{8\pi} s_{iklm} p_{nplm} E_n E_p = \gamma_{iknp} E_n E_p \quad (8)$$

where the tensor \mathbf{s} is reciprocal to the elasticity tensor Λ , and γ is the electrostriction tensor as in the expansion (6). For cubic symmetry this tensor exhibits three independent coefficients γ_{1111} , γ_{1122} and γ_{1212} which could be determined from experimental results as represented in Figure 7. From Kossel diagram observations for a system with negative dielectric anisotropy, a relation between γ_{1111} and γ_{1122} was obtained which reveals a constant volume of the unit cell.⁶⁷ Assuming that this relation is valid in general, the components of the electrostriction tensor were also determined from the spectroscopic data for a mixture with positive dielectric anisotropy (CB15/E9) represented in Figure 7a.⁶⁸ However, investigations by F. Porsch and H. Stegemeyer⁵⁴ on a very similar mixture using Kuczynski's rotating crystal method³⁸ indicated a small positive dilation of the unit cell for BP11.

The absolute values of the electrostriction coefficients are of the order of 10^{-15} – 10^{-14} m²/V², indicating a relative change of the interplanar distances of several per cent if voltages of 10–100V (rms) are applied to a sample with the thickness of 10 μ m. In agreement with considerations by V. E. Dmitrienko,⁷¹ the signs of all components of the electrostriction tensor are reversed if the dielectric anisotropy changes sign (Table II).

The space groups describing the deformed structures are subgroups of the respective cubic space group (I4₃2 or P4₃2) and depend on the direction of the electric field.⁴⁹ Under the influence of an electric field, only the symmetry elements

TABLE II

Sign of the electrostriction coefficients, depending on the sign of the dielectric anisotropy

| | $\epsilon_a > 0$ | | $\epsilon_a < 0$ | |
|-----------------|------------------|-------|------------------|-------|
| | BP I | BP II | BP I | BP II |
| γ_{1111} | - | + | + | - |
| γ_{1122} | + | - | - | + |
| γ_{1212} | + | + | - | - |

consistent with the rotation symmetry of the point group $D_{\infty h}$ (the point group of the dyad $E_i E_j$) are conserved. Thus, the space group of the deformed structure can exhibit only twofold axes perpendicular to the field direction, and no rotational axes oblique to the field direction, whereas the rotational symmetry along the field direction is preserved. Consequently, a field applied along a fourfold, threefold or twofold axis leads to a tetragonal, trigonal or orthorhombic structure, respectively.⁴⁹

2. Change of the Average Molecular Orientation

2.1. Change of the dielectric permittivity. Measurements of the capacitance of blue phase cells as a function of the applied voltage which were performed for both systems with positive^{65,72} and with negative dielectric anisotropy⁶⁵ indicate that the component of the average dielectric permittivity along the field direction

$$\hat{\epsilon} = \frac{1}{|E|^2 V} \int_V E \cdot \epsilon^d(r) E dr^3 \quad (9)$$

increases continuously with increasing field strength. This change indicates that the isotropic distribution of molecular orientation is lost under the influence of the electric field due to the deformation of the blue phase structure.

In order to describe the magnitude of this effect, one might use the ratio ζ between the field-induced change of $\hat{\epsilon}$ in the blue phase and the maximum value of this change expected for the completely unwound structure

$$\zeta = \frac{\hat{\epsilon}_{BP}(E) - \hat{\epsilon}_{BP}(0)}{\epsilon_{||} - \epsilon_{iso}} = \frac{3}{2} \frac{\hat{\epsilon}_{BP}(E) - \hat{\epsilon}_{BP}(0)}{\epsilon_a} \quad (10)$$

For systems with positive dielectric anisotropy ζ is positive and becomes 1 for infinite field strength. For systems with negative dielectric anisotropy ζ is negative and becomes $-1/2$ for infinite field strength when the cholesteric phase in the Grandjean texture is induced ($\epsilon = \epsilon_{\perp}$).

For weak electric fields where the Bragg wavelengths indicate continuous deformation of the blue phase structure, this quantity is proportional to E^2 :

$$\zeta = \zeta_o \cdot E^2 \quad (11)$$

where the magnitude of the factor ζ_o is $1.0 - 2.0 \cdot 10^{-15} \text{ m}^2 \text{V}^{-2}$ ($-0.5 - -1.5 \cdot 10^{-15} \text{ m}^2 \text{V}^{-2}$) for mixtures with positive (negative) dielectric anisotropy.⁶⁵ The absolute value of ζ_o was found to increase with decreasing temperature, i.e. $\zeta_{\text{BPI}} > \zeta_{\text{BPII}}$.

With respect to the symmetry of the tensor order parameter, the dependence of the dielectric tensor on the electric field strength can be described^{57,73,74} by the expansion

$$\epsilon_{ij}(E) = \epsilon_{ij}^{(0)} + \epsilon_{ijk}^{(1)} E_k + \epsilon_{ijkl}^{(2)} E_k E_l + \dots \quad (12)$$

where $\epsilon_{ijk}^{(1)}$ and $\epsilon_{ijkl}^{(2)}$ are tensors of third and fourth rank respectively which must be invariant under the symmetry operations of the respective space group at zero field. $\epsilon^{(1)}$ vanishes for the crystal class O (432) and $\epsilon^{(2)}$ exhibits the form

$$\epsilon_{ijkl}^{(2)} = A \sum_{m=1}^3 n_i^{(m)} n_j^{(m)} n_k^{(m)} n_l^{(m)} + B (\delta_{ij} \delta_{kl} + \delta_{ik} \delta_{jl} + \delta_{il} \delta_{jk}) \quad (13)$$

where $n^{(1)}$, $n^{(2)}$, $n^{(3)}$ are unit vectors along the fourfold axes and A , B are constants.^{57,74} In blue phases the first term is dominating ($|A| \gg |B|$) while the second (isotropic) tensor is relevant for the pretranslational behaviour in the isotropic phase (Kerr effect).

This nonlinear dielectric behaviour in the isotropic phase close to the isotropic-BP phase transition effect was investigated by J. Ziolo *et al.*⁷⁵ In cholesteryl oleate, a pretranslational effect described by the relation $\epsilon(E) - \epsilon(O) \propto E^2/(T - T^*)$ was observed with $T^* = T_{\text{BP-I}} - 0.55^\circ \text{C}$ and $\Delta\epsilon/E^2 \approx 10^{-18} \text{ m}^2 \text{V}^{-2}$ a few $^\circ \text{C}$ above the clearing point.

2.2. Variation of the refractive index, field-induced birefringence. Nonlinear dielectric behaviour occurs also in the frequency range of visible light, leading to a continuous change of the effective refractive index n for light propagating along the field direction.⁷⁶ The value of n was found to decrease (increase) for mixtures with positive (negative) dielectric anisotropy (Figure 9). The quantity ζ used in Section 2.1. can be also derived from optical measurements according to

$$\zeta = \frac{n_{\text{BP}}^2(E) - n_{\text{BP}}^2(O)}{n_o^2 - n_{\text{iso}}^2} = -3 \frac{n_{\text{BP}}^2(E) - n_{\text{BP}}^2(O)}{n_e^2 - n_o^2} \quad (14)$$

where n_e and n_o are the extraordinary and the ordinary refractive index for the nematic phase occurring in the respective racemic mixture close to the clearing temperature. The effective refractive index corresponds to the isotropic value at zero field, to the ordinary refractive index n_o in the homeotropic nematic state ($\epsilon_a > 0$, $E \rightarrow \infty$) and to the value $n_{ch} = \sqrt{(n_e^2 + n_o^2)/2}$ for light propagating along the helix axis in the cholesteric phase ($\epsilon_a < 0$, $E \rightarrow \infty$). The values for ζ obtained from the data represented in Figure 9 are in good agreement with the numbers given in Section 2.1 which were obtained from dielectric measurements.

Field-induced birefringence for light propagating along the field direction was observed in BPI when the twofold axis is oriented parallel to the field.⁷⁷ Domains

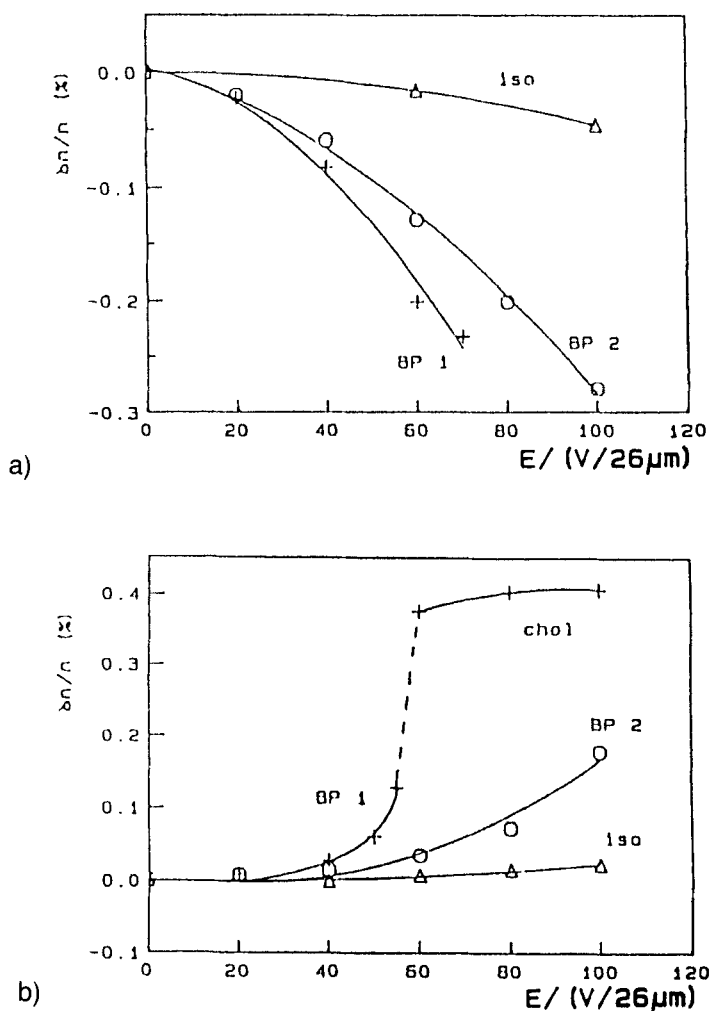


FIGURE 9 Relative change of the mean refractive index (for light propagating along the field direction) under the influence of an electric field a) for a system with positive dielectric anisotropy (62.3% CB15, 37.7% RO-TN404) and b) for a system with negative dielectric anisotropy (26.5% S811, 73.5% EN18). (From G. Heppke *et al.*⁷⁶).

with azimuthal orientations differing by 90°C , which form the typical cross hatching texture,^{78,79} behave like retarders with different azimuthal orientation of their fast axis (Figure 10). This birefringence disappears at the field-induced phase transition to the tetragonal phase BPX (BPEa).⁸⁰

2.3. Dye guest-host-effect in blue phases. It is well known that rodlike dye molecules (guest) dissolved in a liquid crystal (host) are preferably oriented with their long axes parallel to the director. This effect was used to realize twisted nematic displays without any polarizers,⁸¹ and it was also studied in smectic phases for application in ferroelectric displays.⁸² For light transmitted through such guest-

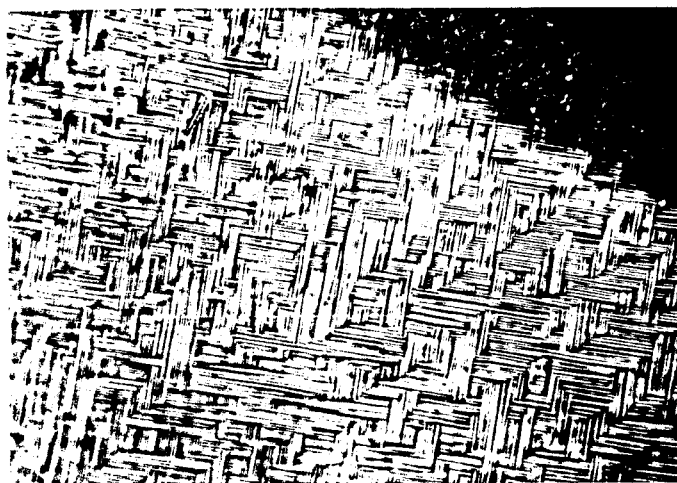


FIGURE 10 Cross-hatching texture of BPI showing electric field induced birefringence (mixture of the compounds CPMBB and CBMBB).

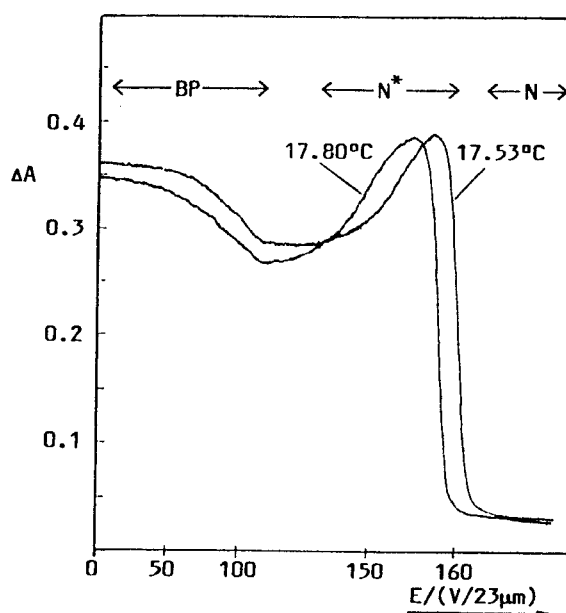


FIGURE 11 Absorbance versus field strength for a dye guest host blue phase mixture (62.3% CB15, 37.7% ZLI 1841).

host mixtures maximum absorbance is observed if the plane of polarization of light is parallel to the director, whereas minimum absorbance occurs if the director is oriented perpendicular to the plane of polarization (e.g. for light of any polarization propagating parallel to the director).

This guest host effect can also cause a change of the absorbance in blue phase mixtures due to the change of the mean molecular orientation under the influence of an electric field.⁸³ In a mixture with positive dielectric anisotropy containing three dichroic dyes, a continuous decrease of the intensity of transmitted light was observed with increasing field strength in the blue phase range (Figure 11). For a field strength where the cholesteric phase is induced, the sample becomes opaque due to diffuse scattering. At higher field strength the nematic state is induced, where the sample becomes transparent (Figure 11).

3. Orientation of Single Crystals

Single crystals of BPI and BPII which are grown in the electric field were found to be oriented with one of their fourfold axes parallel to the field direction. Reorientation to this most stable orientation was observed for randomly oriented single crystals in materials with positive⁶⁷ as well as for materials with negative dielectric anisotropy.⁶⁷ However, single crystals anchored at the glass surface of a sample were found to be metastable when one of their twofold or threefold axes are perpendicular to the surface.

According to P. Pieranski *et al.*,⁵⁷ the orientation of single crystals can be considered theoretically by regarding the torque $\Gamma = \mathbf{V}(\mathbf{P} \times \mathbf{E})$ acting on a cubic single crystal. Since only the nonlinear, anisotropic part of the polarizability contributes to this torque, i.e. the second term in Equation (13), the torque was shown to be of the general form

$$\Gamma = \mathbf{V} A \sum_{i=1}^3 (n^{(i)} \cdot \mathbf{E})^3 (n^{(i)} \times \mathbf{E}) \quad (15)$$

(where the quantities A , $n^{(1)}$, $n^{(2)}$, $n^{(3)}$ have the same meaning as in Equation (13)). This expression vanishes for the orientations $[001] \parallel \mathbf{E}$, $[011] \parallel \mathbf{E}$ and $[111] \parallel \mathbf{E}$. Either the orientation $[001] \parallel \mathbf{E}$ (for $A > 0$) or the orientation $[111] \parallel \mathbf{E}$ (for $A < 0$) is absolutely stable.

The same result was also obtained by D. Lubin and R. M. Hornreich⁷⁴ by minimization of the free energy. The most stable orientation is $[001] \parallel \mathbf{E}$ for the space groups $P 4_232 (O^2)$ and $I 4_132 (O^8)$ and $[111] \parallel \mathbf{E}$ for the space group $I 432 (O^5)$.⁷⁴ In this most stable orientation, the decrease of the free energy with applied voltage is proportional to E^4 .

The reorientation under the influence of an electric field can be observed also macroscopically by investigation of the selective reflection of a polycrystalline sample for an area of the sample surface which is large compared to the size of the platelets. Due to reorientation, the intensity for the (100) peak in BPII and the (200) peak in BPI increases, while the intensities for other Bragg peaks decrease, respectively. An interesting exception occurs for BPI in mixtures with positive dielectric anisotropy. F. Porsch and H. Stegemeyer⁸⁴ observed a disappearance of the (200) peak under the influence of an electric field. The occurrence of the (110) selective reflection after the voltage was removed, indicated a uniform orientation of BPI with one of its twofold axes perpendicular to the sample surface. Since this

behaviour, being in contradiction to observations in other systems,⁵⁷ was observed only in a mixture showing the field-induced tetragonal phase BPX,^{55,80} it was concluded that the disappearance of the (200) peak of BPI is due to the transition to the field induced tetragonal blue phase BPX (BPEa). It was argued^{85,86} that the orientation of BPI with its twofold [110] axis along the field direction on decreasing field strength is due to the continuous transformation of the BPX lattice into the lattice of the deformed BPI, as described in the next paragraph.

4. Field-induced Phase Transitions

Detailed investigations of blue phase single crystals by means of orthoscopic microscopy and by studying Kossel diagrams reveal a rich polymorphism of blue phases. A tetragonal blue phase BPX^{55,87} (Figure 12a), a three dimensional hexagonal phase BPH^{3D},⁸⁷ and a two dimensional hexagonal phase BPH^{2D}⁸⁸ can occur under the influence of an electric field in addition to BPI, BPII and BPIII. F. Porsch and H. Stegemeyer introduced the names BPE,⁸⁰ or BPEa, BPEb and BPEc⁸⁹ for the field-induced phases observed in their mixtures. By comparison of the topology of the phase diagrams given by P. Pieranski *et al.*^{35,87} and by N.-R. Chen and J. T. Ho⁹⁰ with the phase diagrams given by F. Porsch and H. Stegemeyer^{80,89} one can conclude the identities “BPX” = “BPEa” and “BPH^{2D}” = “BPEc”. The structure of a further field-induced blue phase, BPEb⁸⁹ (Figure 12b), is not yet identified. For completeness it should be mentioned that the name ‘BPE’ (which corresponds to the tetragonal blue phase in Reference 80) is also used by other authors^{91,92} for any field-induced blue phase structure being not identified.

P. Pieranski *et al.*⁸⁷ found for a mixture with positive dielectric anisotropy that the discontinuous increase of the Bragg wavelength on increasing electric field strength observed by G. Heppke *et al.*⁶² correspond to a field-induced phase transition from BPII to a tetragonal phase BPX which differ not only in its lattice constant from BPII but also in the shape of its single crystals (Figure 12a). By investigation of Kossel diagrams⁵⁵ it was shown that BPI oriented with its twofold axis along the field direction can be also transformed to BPX, but without a discontinuous change of the interplanar distance of the planes perpendicular to the electric field. The Kossel lines observed for BPX indicate a centered tetragonal structure.⁹³ It was concluded that the space group of BPX is $I 4_122$ since the unit cell of this space group can be obtained continuously by shearing the orthogonal $F 222 (D_2^7)$ unit cell which describes the deformed BPI lattice (Figure 13).

The three dimensional hexagonal phase BPH^{3D} occurs in materials both with $\epsilon_a > 0$ ⁸⁷ and with $\epsilon_a < 0$.⁹⁴ For systems with $\epsilon_a > 0$, a transition from BPX to BPH^{3D} can be observed on increasing field strength which is connected with a discontinuous decrease of the selective reflection wavelength.⁹³ For mixtures with $\epsilon_a > 0$ exhibiting very high chirality and for mixtures with $\epsilon_a < 0$ (in which no BPX has yet been observed, Figure 12c), a continuous transition from BPII to BPH^{3D} occurs. According to the selection rules for three dimensional hexagonal space groups,³⁵ the Kossel diagrams for BPH^{3D} are in agreement with one of the space groups $P 6_222$, $P 6_422$, $P 6_2$ or $P 6_4$. However, the continuous transition from the deformed BPII (BPII^d) to BPH^{3D} gives evidence for the space groups $P 6_222$ or $P 6_422$. For these space groups the transition from BPII^d ($P 4_222$) to BPH^{3D} can be described by a



Downloaded by [Tomsk State University of Control Systems and Radio] at 09:46 19 February 2013

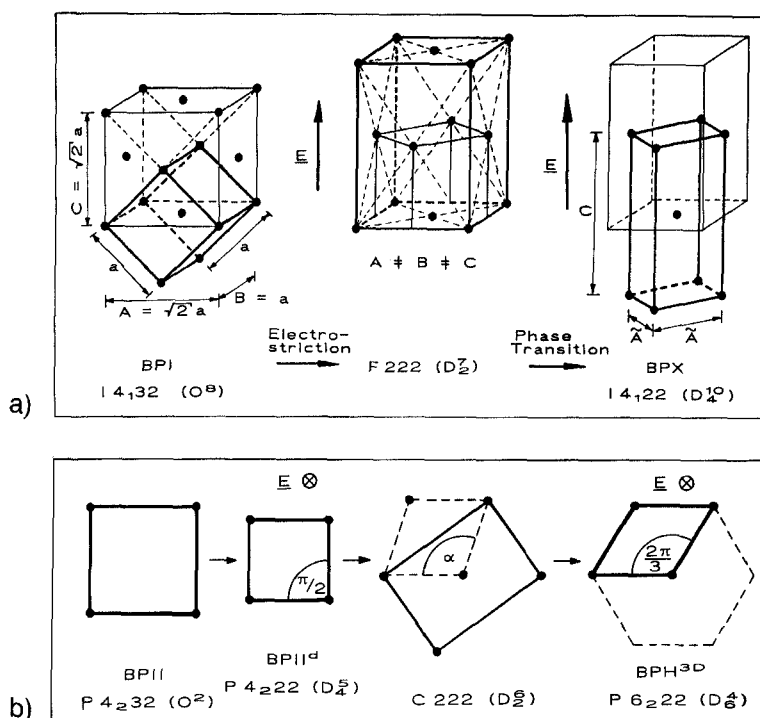


FIGURE 13 Transformation of the unit cells for the phase transitions a) BPI-BPX and b) BPII-BPH^{3D} which are not connected with a discontinuity of the interplanar spacing along the field direction.

shear of the $P 4_2 22$ unit cell of BPII^d transforming the lattice via the subgroup $C 222$ continuously to the structure of BPH^{3D}.

The occurrence of a two-dimensional hexagonal phase BPH^{2D} (BPEc) was experimentally observed for mixtures of high chirality with $\epsilon_a > 0$.⁸⁸ This structure is always oriented with its sixfold axis parallel to the field direction and thus exhibits no Bragg reflection when observed along this direction. Consequently, dark single crystals were observed⁸⁸ and the Kossel diagrams of BPH^{2D} consist only of six straight lines which correspond to the reciprocal lattice vectors perpendicular to the field direction.

It is interesting to note that the stability of a hexagonal structure with respect to the cholesteric phase (also at zero field) was proposed as early as 1975 by S. A. Brazovskii and S. G. Dmitriev⁹⁵ using a Landau theory. G. Sigaud¹³ who was the first observing any faceted blue phase single crystal (presumably a crystal limited by (110) facets oriented with a twofold or threefold axis along the viewing direction), concluded from its hexagonal shape erroneously that blue phases are hexagonal (at zero field). After the cubic structures of BPI and BPII were established, the additional occurrence of a two dimensional hexagonal phase in the field was predicted theoretically by R. M. Hornreich and S. Shtrikman.^{96,97} However, the first hexagonal structure being observed experimentally was BPH^{3D},⁸⁷ and only later BPH^{2D} was found additionally.⁸⁸ By more recent experiments evidence was given for the occurrence of BPH^{3D} also in systems with negative dielectric anisotropy⁹⁴

(Figure 12c). Phase diagrams obtained by Landau theory^{98,99} (Figure 12d) show in good agreement with experiments that BPH^{3D} becomes stable in the electric field for materials with both positive and negative dielectric anisotropy, that BPH^{2D} occurs for materials with positive dielectric anisotropy at higher field strength than BPH^{3D}, and that the occurrence of BPH^{3D} requires high chirality of the system.³⁵

The detailed investigation of the dependence of the transition field strengths on the chirality by B. Jérôme and P. Pieranski³⁵ (Figure 14) might give an explanation why in some mixtures^{62,87,90} a discontinuous change of the Bragg wavelength on increasing voltage was observed in the temperature interval of BPII (due to the transition BPII-BPX) whereas in mixtures with very similar composition but slightly different concentrations^{4,73,80} no such discontinuity was detected (because the transition BPII-BPH^{3D} is continuous). Figure 14 shows also that the threshold value for the unwinding of the blue phase structure to the cholesteric phase increases with increasing chirality. For a system with a very large temperature dependence of the cholesteric pitch this dependence was found to lead to a reentrancy of the cholesteric phase.¹⁰⁰ The space groups describing the structures occurring due to electrostriction or due to field-induced phase transitions are summarized in Figure 15. A summary of references is given in Table III.

According to the field dependence of the free enthalpy,¹⁰¹ the transition lines in

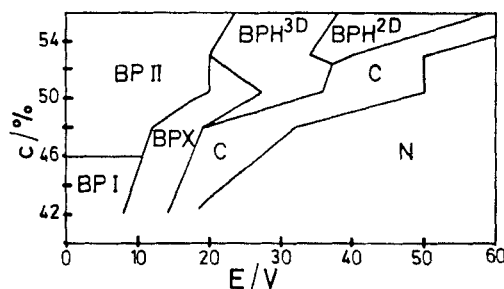


FIGURE 14 Phase diagram in the (electric field, chirality) plane. c is the concentration (by weight) of the chiral compound CB15 in mixtures with the nematic material E9. Indicated are the phases appearing in the temperature region just below the clearing temperature. (From B. Jérôme and P. Pieranski³⁵).

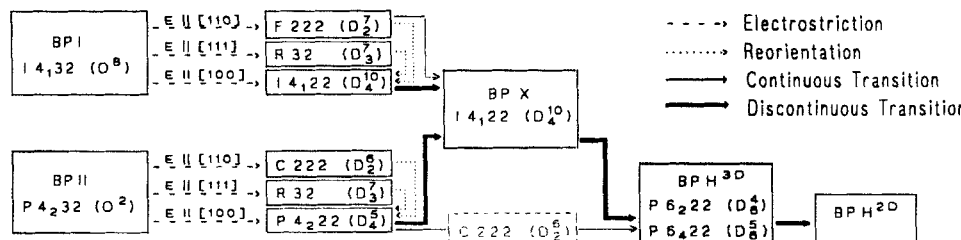


FIGURE 15 Space groups describing the continuously deformed structures of BPI and BPII and the field-induced BP modifications.

an electric field–temperature phase diagram have to fit in a Clausius-Clapeyron type of relation

$$\frac{dT}{dE} = - \frac{\Delta P}{\Delta S} \quad (16)$$

where ΔP is the difference between the dielectric polarizations of the respective phases and ΔS is the difference of their entropy. As far as these transitions can be considered as a shift of the transition temperature, this temperature shift is given by the integrated form of Equation (16)

$$\Delta T = T - T_o = - \frac{M T_o}{\rho \Delta H_m} \epsilon_o \int_0^E \Delta \hat{\epsilon} E' dE' \quad (17)$$

A similar relation derived by W. Helfrich¹⁰² for the case that $\hat{\epsilon}_I$ and $\hat{\epsilon}_{II}$ are independent on the field strength. Helfrich's equation was used by C. Motoc and M. Honciuc¹⁰³ and by H. Stegemeyer *et al.*⁷³ to discuss the transition BP-N*. A paper by B. Spier and H. Stegemeyer¹⁰⁴ is devoted to the hysteresis of this transition.

5. Facetting of Single Crystals Grown in an Electric Field

The shape of BP single crystals can be affected considerably by the influence of an electric field, as found by P. Pieranski *et al.*^{105,106} Single crystals of BP_{II} are usually limited by (110) and equivalent facets and thus show a quadratic shape when observed along one of their fourfold axes. However BP_{II} crystals grown in an electric field with their [001] axis parallel to E form an octogon indicating an additional occurrence of (100) facets.

The different growth rates of the respective facets (hkl) were discussed assuming two dimensional nucleation of steps on the crystal surface. In this model the growth rate decreases exponentially with the height of the nucleation barrier which is proportional to the energy per unit length $\beta(hkl)$ of a step.¹⁸ It was shown that the dependence of this quantity on the applied electric field is described by $\beta \propto E \cdot d^{3/2}$ where d is the period of the spatial modulation of the dielectric energy perpendicular to the respective planes. Consequently, lateral (100) surfaces parallel to the field appear in BP_{II}, since $\beta(100) > \beta(110)$ and thus the growth rate along the [100] direction becomes smaller in an electric field than the growth rate along the [110] direction. For BP_I, however, where the longest periodicity along the [100] direction perpendicular to the field is $a/2$, no additional (200) facets occur since $\beta(200) < \beta(110)$.

More recently it was shown¹⁰⁶ that also facets which are equivalent in a cubic single crystal, can exhibit different growth rates in the presence of an electric field. Thus, single crystals of BP_{II} grown in an electric field show reduced symmetry compared to those crystallites grown without field (Figure 16), which demonstrates that the field breaks the spatial isotropy. This effect which is very small for atomic crystals, could be clearly observed in blue phase crystals.

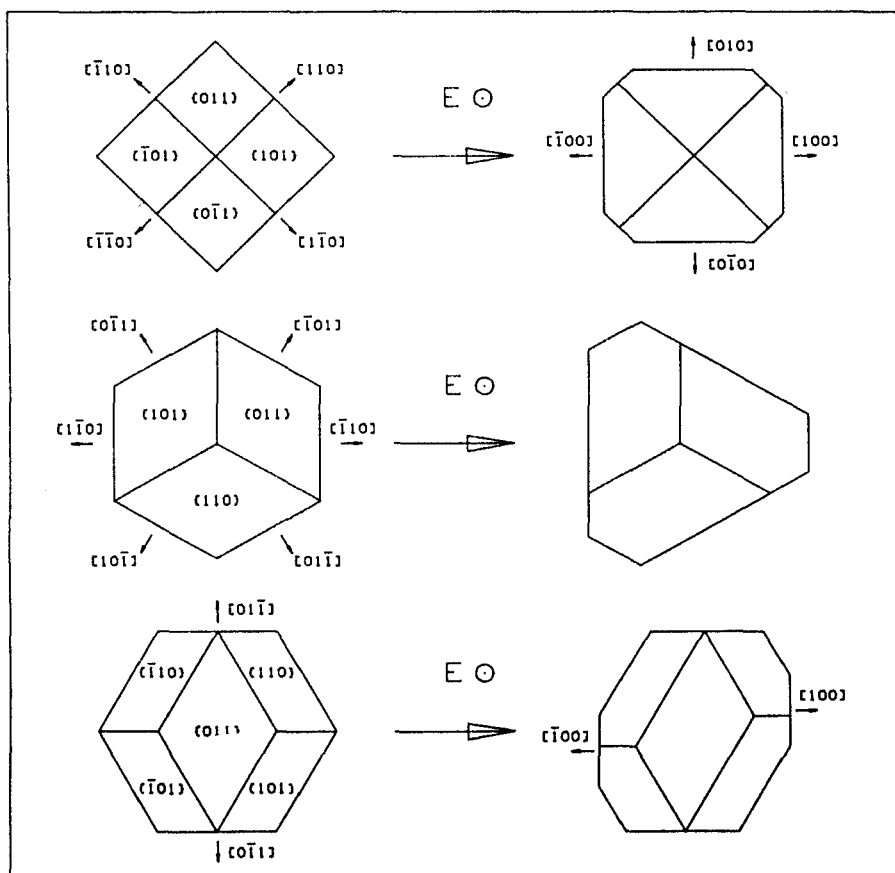


FIGURE 16 Shape of BP11 single crystals a) without and b) with an applied electric field $E \parallel [001]$, c) $E \parallel [111]$, d) $E \parallel [011]$, according to the considerations by P. Pieranski *et al.*¹⁰⁶

The symmetry of a crystal grown in the field is described by a point group which must be a common subgroup both of the point group O of the crystal structure and of the point group $D_{\infty h}$ describing the axial symmetry induced by the field. Thus, crystals oriented with one of their fourfold, threefold or twofold axes oriented along the field direction exhibit shapes with the symmetry D_4 , D_3 and D_2 , respectively. As a consequence, it was observed¹⁰⁶ that the set of 12 equivalent (110) facets limiting a single crystal of BP11 split into several subsets which differ in their growth rate (Figure 16). For $[001] \parallel E$ two subsets of facets occur (8 planes equivalent to (101) ; 4 planes equivalent to (110)), for $[111] \parallel E$ three different subsets (6 planes equivalent to (110) , 3 planes equivalent to $(\bar{1}10)$ and 3 planes equivalent to $(\bar{1}01)$), and for $[011] \parallel E$ four different subsets (4 planes equivalent to (110) , 4 planes equivalent to (101) , 2 planes equivalent to (011) and 2 planes equivalent to $(0\bar{1}1)$). The growth rates of these facets were also discussed extensively in terms of the energy $\beta(110)$ of steps nucleating on the surfaces of a crystal.¹⁰⁶

III. ELECTRIC FIELD EFFECTS IN BPIII

In contrast to BPI and BP II, the modification BPIII exhibits a very broad selective reflection band of very low intensity.⁴⁵ The very small latent heat for the transition BP II-BPIII seems to indicate that the small scale structure of BPIII is very similar to BPI and BP II, i.e. characterized by double twist. The linewidth data, however, indicate that the size of correlated regions in the BPIII structure is only a few pitches.^{46,91} Different models were proposed to describe the structure of this modification. According to the emulsion model,⁶¹ BPIII is considered as an emulsion of cholesteric droplets in an isotropic matrix, the double twist model¹⁰⁷ consists of randomly oriented double twist cylinders, the cubic domain model^{108,109} contains small body centered cubic or simple cubic domains or correlated regions, and the quasicrystal model^{110–112} is locally characterized by a reciprocal lattice with icosahedral symmetry.

The behaviour of BPIII in an electric field was found to be considerably different to BPI and BP II. In systems with $\epsilon_a > 0$ a decrease of the intensity of the selective reflection (Figure 17a) and a small shift of the peak to larger wavelength were observed by D. K. Yang and P. P. Crooker.⁹¹ In mixtures with $\epsilon_a < 0$, however, the peak of the selective reflection shows a large increase of the intensity and a sharpening under the influence of an applied field (Figure 17b).^{113,114} The selective reflection peak is slightly shifted to smaller wavelengths for $\epsilon_a < 0$. From linewidth data given for materials with $\epsilon_a < 0$, one can conclude that the size of the scattering domains $L \approx \lambda^2/(\pi n \Delta \lambda)$ increases with increasing field strength from about 300 nm to about 2 μm for these materials.¹¹⁵ These field effects in BPIII were discussed with respect to the different models for the BPIII structure. In the following paragraphs, a brief summary of the arguments is given.

In principle, the behaviour of BPIII in an electric field is consistent with the emulsion model and the double twist model. Since the reciprocal lattice vectors along the helix axis of a cholesteric structure are favorably aligned parallel to the field direction for materials with $\epsilon_a < 0$ and perpendicular to the field for systems with $\epsilon_a > 0$, the respective reorientation of cholesteric droplets would cause an intensity increase for $\epsilon_a < 0$ and an intensity decrease for $\epsilon_a > 0$, as observed experimentally. Qualitatively, the same arguments are valid for double twist cylinders orienting parallel to E for $\epsilon_a > 0$ and perpendicular to E for $\epsilon_a < 0$. However, in contrast to the effects of reorientation in BPI and BP II, the intensity change in BPIII is reversible.^{113,114}

With respect to the cubic domain model, the results on electric field effects seem to argue against the space group $I 432 (O^5)$ as well as against BP II like $P 4_232 (O^2)$ or BPI like $I 4_132 (O^8)$ domains. In the first case the structure exhibits only (110) reciprocal lattice vectors. The increase of intensity observed for BPIII in systems with $\epsilon_a < 0$ would indicate a reorientation of the lattice leading to an alignment of the twofold axis parallel to the field. However, this orientation was shown to be only metastable for all cubic space groups.^{57,74} For cubic domains with $I 4_132 (O^8)$ or $P 4_232 (O^2)$ structure, a reorientation with the fourfold axis parallel to the field like in BPI and BP II would be expected for both systems with positive and negative dielectric anisotropy. This is in contradiction to the observation that BPIII

TABLE III

Field-induced phase transitions observed experimentally. The part of this table above its diagonal corresponds to systems with $\epsilon_a > 0$, the part below the diagonal correspond to materials with $\epsilon_a < 0$. (< . . >): Respective references, o: not yet observed. ?: It is not yet clear, whether the field-induced phase ("BPE" in Reference 113,115) occurring in the temperature range of BPIII is identical to BPII (as assumed in Reference 120,121) or to BPH^{3D}

| | BPIII | BPII | BPI | BPX BPE _a | BPE _b | BPH ^{3D} | BPH ^{2D} BPE _c | N [*] | N |
|---------------------------------------|------------------|---------------------------|---------------|-------------------------|------------------|---------------------------|---------------------------------------|--|--------|
| BPIII | - | <91>? <120>? <121>? | o | o | o | <91>? <120>? <121>? | o | o | o |
| BPII | <113>? <115>? | - | <90> | <87,90> <93,35> | o | <35> | <89> | <80,90> <73> | <120>? |
| BPI | o | o | - | <55,93> <80,35> | o | o | o | <60,61> <62,90> <89,73> <100> | o |
| BPX BPE _a | o | o | o | - | <89> | <87,90> <93,35> | o | <88,35> <80,89> | o |
| BPE _b | o | o | o | o | - | o | o | <89> | <89> |
| BPH ^{3D} | <113>? <115>? | <94> | <94> | o | o | - | <88,35> | <87,90> <35> | <120>? |
| BPH ^{2D} BPE _c | o | o | o | o | o | o | - | <88,35> | <89> |
| N [*] | o | <66> <104> | <66> <104> | o | o | <94> | o | - | <129> |
| N | - | - | - | - | - | - | - | - | - |

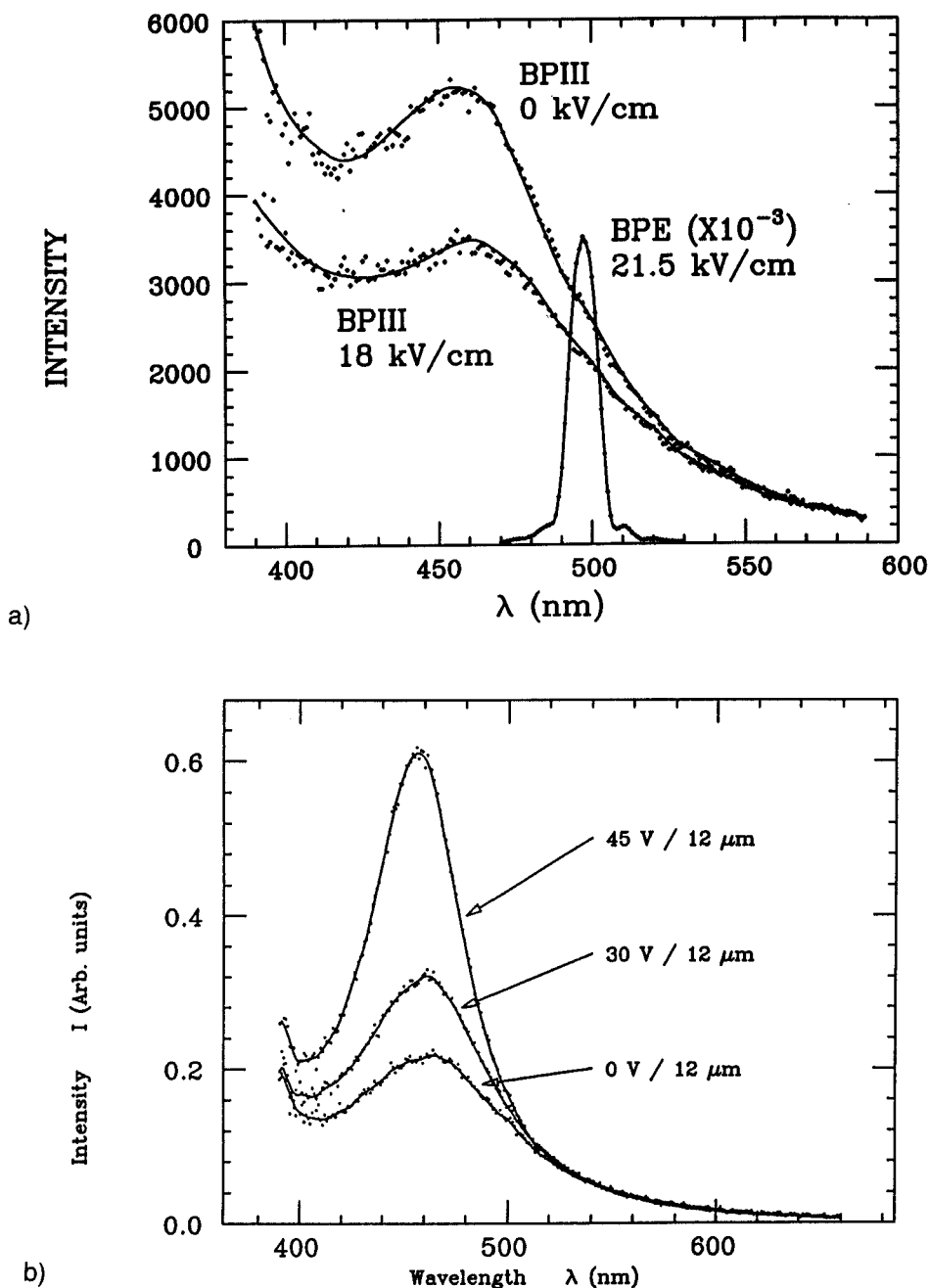


FIGURE 17 Reflected intensity versus wavelength in the temperature range of BPIII for several electric field strengths. a) Mixture with positive dielectric anisotropy (17.6% CE1, 28.1% CE2, 54.3% K18, $T = 81.041^\circ\text{C}$). (From D. K. Yang and P. P. Crooker.⁹¹) b) Mixture with negative dielectric anisotropy (30.0% S811, 70.0% EN18, $T = 44.052^\circ\text{C}$).¹¹⁴

behaves distinctly different in the electric field depending on the sign of ϵ_a . However these arguments do not exclude the cubic domain model in general since for other cubic space groups which were not taken into consideration so far, the absolutely stable orientation might be $[111] \parallel E$ for $\epsilon_a > 0$ and $[001] \parallel E$ for $\epsilon_a < 0$. In the latter case, the change of the intensity observed experimentally would be in agreement with the reorientation. Another argument against the cubic domain model and against the quasicrystal model was given by D. K. Yang, P. P. Crooker and K. Tanimoto.¹¹⁶ According to their observation, BPIII can be surface aligned but the higher harmonics expected for these structures could not be observed by rotating the sample.

With respect to the quasicrystal model, no detailed theoretical predictions on electric field effects were published so far. However, according to recent considerations by V. E. Dmitrienko,¹¹⁷ it should be possible to distinguish between the double twist model (or the emulsion model), the cubic domain model and the quasicrystal model, by careful analysis of the dependence of the BPIII linewidth in systems with $\epsilon_a < 0$ on the electric field strength. Thus, the behaviour of these systems is presently under more precise investigation.¹¹⁸

For systems with $\epsilon_a > 0$ as well as for systems with $\epsilon_a < 0$, a field induced transition from BPIII to BPE was observed^{91,113,114} (Table III) where BPE is a field-induced blue phase modification identical either with the continuously deformed BPII or with BPH^{3D}. Thus, the intensity increase in BPIII for $\epsilon_a > 0$ might be considered as a pretransitional effect for the field-induced transition to the BPE.

IV. DYNAMICS

Preliminary measurements of the time constants for the electric field effects in BPI and BPII by G. Heppke *et al.*⁷⁶ indicated that the time constants for the electrostriction (several seconds) and for the field-induced change of the refractive index ($\approx 1\text{ms}$) differ by several orders of magnitude. P. R. Gerber¹¹⁹ found even time constants of about 100 μs for the change of the refractive index. A similar fast response was reported by H. J. Coles and H. F. Gleeson^{120,121} who observed the integrated intensity reflected from blue phase samples.

More precise measurements on the dynamics of the comparably slow electrostriction were performed recently¹¹⁵ using time resolved spectroscopy. In the case of BPI, the Bragg wavelengths as a function of time were well fitted by a sum of two exponentials, the time constants being of the order of several tenth of a second and several seconds, respectively. For BPII, the time dependence of the Bragg wavelength corresponding to the (100) planes was well fitted by a single exponential¹¹⁵ with a time constant of about 3 s.

In order to describe the dynamic behaviour theoretically, the equation of motion was considered¹²² to be of the form

$$\mu(\dot{v} - \ddot{u}) + \Lambda \nabla^2 u = 0 \quad (18)$$

where v is the velocity of the background fluid and μ is a permeation coefficient.

Using the approximations that the background fluid is at rest ($v = 0$) and that the boundary conditions do not restrict the director configuration, solutions to Equation (18) for the case of only one dimension are given¹¹⁵ by

$$u(x) = \sum_n [A_n e^{-x/t_n}] \sin(q_n x) \quad (19)$$

where $q_n = n\pi/L$ and $t_n = \mu/\Lambda q_n^2$. The length L characterizes the size of the strained lattice, i.e. L may correspond to the diameter of the BP single crystals or to the sample thickness, depending on the experimental conditions. Taking $\Lambda \sim K_2 q_0^2$ and $\mu \sim \nu_1 q_0^2$ (in analogy with the permeation constant introduced by W. Helfrich¹²³), P. P. Crooker¹¹⁵ derived the expression

$$t_1 = \frac{\nu_1}{K_2 q_1^2} \quad (20)$$

for the magnitude of the largest time constant t_1 , where ν_1 is the twist viscosity and K_2 is the twist elastic constant. Using $\nu_1 = 1 \text{ dyn s/cm}^2$, $K_2 = 5 \cdot 10^{-7} \text{ dyn}$ and $L = 12 \text{ }\mu\text{m}$, the time constant was estimated to be about 0.3 s, which is about one order of magnitude less than the experimental electrostriction times. This discrepancy and the observation of Cano steps in some of the investigated blue phase samples, indicate that in fact the boundary conditions might have a significant influence on the dynamics of electrostriction.

The two step mechanism indicated by the different time constants for the change of the refractive index and for the electrostriction is comparable to the helical unwinding of the cholesteric phase. Recent considerations by R. M. Hornreich¹²⁴ give a small time constant of $t_s = \nu p_0^2/(16\pi^2 K_2)$ for the generation of higher harmonics (which corresponds to a change of the refractive index) and a large time constant $t_l = \nu L^2/(3K_2)$ for the change of the cholesteric pitch. The time constants estimated by using typical values for the twist viscosity ν_1 , for the cholesteric pitch p and for the sample thickness L , exhibit a similar magnitude as the different time constants found for the refractive index change and the electrostriction in BPI and BP II.

For intensity change of the reflectivity in BP III, time constants of the order of ms were measured.¹¹⁵ It was concluded that the behaviour of BP III in electric fields is fundamentally different from the electrostriction of BPI and BP II. However, to give an estimate of the time constant of this effect, one might use equation 20 (although this equation was derived for the electrostriction) and substitute the sample thickness L ($= 12 \text{ }\mu\text{m}$) by the size of the BP III domains ($\approx 1 \text{ }\mu\text{m}$). In this case, a time constant of 2 ms is obtained from Equation 20. It is remarkable that the time constants t_{on} for the switching on process were found to be larger than for the switching off process, and that t_{on} increases with increasing field strength for BP III. This behaviour differs from the majority of electrooptical effects in liquid crystals.¹²⁵ However, according to the application of Equation 20, this result is in qualitative agreement with an increase of the domain size with increasing voltage, as indicated by the sharpening of the peak.

V. CONCLUSION

The preceding review was focussed on the electric field effects in blue phases. During the last decade, continuous changes of the blue phase structure, reorientation and deformation of blue phase single crystals and field-induced phase transitions revealing a rich polymorphism of blue phases were investigated. Some of these effects, especially the shift of the Bragg-wavelengths, the change of the refractive index or the dye guest host effect, might be interesting for applications, provided that it would be possible to enlarge the blue phase temperature range by one order of magnitude.

Although the behaviour of BPI and BPII in electric fields is well investigated, there are still interesting questions to solved. While the field-induced phases BPEa and BPEc⁸⁹ can be identified with the tetragonal BPX and the hexagonal structure BPH^{2D}, respectively, the structure of the field-induced modification BPEb occurring in systems with positive dielectric anisotropy is still unknown. Moreover, it seems of interest to study more systems with negative dielectric anisotropy in order to investigate whether BPEb or the tetragonal phase BPX (BPEa) occurs also in these systems. Investigations on the statics and on the dynamics of electric field effects in BPIII might give additional informations on this unknown structure. However, both theoretical predictions and more precise experimental data have to be obtained in order to determine the structure of BPIII. Additional informations concerning this question might be obtained from NMR experiments.^{126,127}

Besides the influence of electric fields, it might be also interesting to study distortions, symmetry breaking or phase transitions of blue phase structures by other parameters. In 1983, C. Motoc and M. Honciuc¹⁰³ observed that the nucleation of the cholesteric phase from a supercooled blue phase can be influenced by a magnetic field. While the helical unwinding of the cholesteric phase is well known for both magnetic¹²⁸ and electric fields,¹²⁹ only few work was done yet on magnetic field effects in blue phases. However only small effects should be expected by available magnetic fields, since the complete unwinding of a cholesteric phase with $p = 500$ nm and $\chi_a = 10^{-7}$ ¹²⁵ would require a field strength of 60 Tesla. A. I. Feldman *et al.*¹³⁰ found that uniaxial strain occurring in a Cano wedge can cause apart from changes of the lattice constant also a shift of transition temperatures, and even a reentrancy in blue phases. Thus, it seems to be promising to study also the influence of boundary conditions and of mechanical stress on blue phase structures in more detail.

Acknowledgment

The author would like to thank G. Heppke, P. Pieranski, B. Jérôme, P. P. Crooker, R. M. Hornreich, V. A. Belyakov, V. E. Dmitrienko and H.-R. Trebin for illuminating discussions. Special thanks are dedicated to my colleagues F. Oestreicher, M. Krumrey, Ch. Papenfuß and H. Schmid for fruitful collaboration and to Th. Krekler for technical assistance concerning the photographs (Figure 6) in this article. This work was supported by the Deutsche Forschungsgemeinschaft (Sonderforschungsbereich 335 'Anisotrope Fluide').

References

1. F. Reinitzer, *Monatshefte Chemie*, **9**, 421 (1888).
2. P. P. Crooker, *Liquid Crystals*, **5** (3), 751–775 (1989).
3. P. E. Cladis in: "Theory and Applications of Liquid Crystals," pp. 73–98, edited by J. L. Ericksen and D. Kinderlehrer, Springer, New York (1987).
4. H. Stegemeyer, Th. Blümel, K. Hiltrop, H. Onusseit, F. Porsch, *Liquid Crystals*, **1** (1), 3–28 (1986).
5. V. A. Belyakov, V. E. Dmitrienko, *Sov. Phys. Usp.*, **28** (7), 535–562 (1985).
6. H.-R. Trebin, *Phys. Bl.*, **44** (7), 221–226 (1988).
7. G. W. Gray, *J. Chem. Soc.*, **1956**, 3733–3739 (1956).
8. A. Saupe, *Mol. Cryst. Liq. Cryst.*, **7**, 59–74 (1969).
9. D. Coates, G. W. Gray, *Phys. Lett.*, **45A** (2), 115–116 (1973).
10. H. Onusseit, H. Stegemeyer, *Z. Naturforsch.*, **39a**, 658–661 (1984).
11. D. L. Johnson, J. H. Flack, P. P. Crooker, *Phys. Rev. Lett.*, **45** (8), 641–44 (1980).
12. S. Meiboom, M. Sammon, *Phys. Rev. Lett.*, **44** (13), 882–885 (1980).
13. G. Sigaud, *Mol. Cryst. Liq. Cryst.*, **41** (Lett.), 129–135 (1978).
14. M. Marcus, *J. Phys. (Paris)*, **42**, 61–70 (1981).
15. H. Onusseit, H. Stegemeyer, *Z. Naturforsch.*, **36a**, 1083 (1981).
16. P. E. Cladis, P. Pieranski, M. Joanicot, *Phys. Rev. Lett.*, **52** (7), 542–5 (1984).
17. R. Barbet-Massin, P. E. Cladis, P. Pieranski, *Phys. Rev. A*, **30** (2), 1161–64 (1984).
18. P. Pieranski, R. Barbet-Massin, P. E. Cladis, *Phys. Rev. A*, **31** (6), 3912–23 (1985).
19. Th. Blümel, H. Stegemeyer, *J. Crystal Growth*, **66**, 163–168 (1984).
20. Some earlier papers^{11,21} contain also hints on a modification BPIIb²¹ showing the same Bragg peaks as BPI but a different temperature dependence of these peaks. According to M. Marcus,²² the respective mixtures exhibit in fact a BPI/isotropic two phase region, but no blue phase modification besides BPI.
21. J. H. Flack, P. P. Crooker, *Phys. Lett.*, **82A** (5), 247–50 (1981).
22. M. A. Marcus, *Mol. Cryst. Liq. Cryst.*, **82** (Lett.), 33–39 (1982).
23. K. Bergmann, H. Stegemeyer, *Z. Naturforsch.*, **34a**, 251–252 (1979).
24. Th. Blümel, P. J. Collings, H. Onusseit, H. Stegemeyer, *Chem. Phys. Lett.*, **116** (6), 529–33 (1985).
25. M. A. Marcus, J. W. Goodby, *Mol. Cryst. Liq. Cryst.*, **72** (Lett.), 297–305 (1982).
26. K. Tanimoto, P. P. Crooker, G. C. Koch, *Phys. Rev. A*, **32** (3), 1893 (1985).
27. R. N. Kleiman, D. J. Bishop, R. Pindak, P. Taborek, *Phys. Rev. Lett.*, **53** (22), 2137–2140 (1984).
28. J. Thoen, *Phys. Rev. A*, **37** (5), 1754–9 (1988).
29. P. Taborek, J. W. Goodby, P. E. Cladis, *Liquid Crystals*, **4** (1), 21–38 (1989).
30. G. Voets, H. Martin, W. Van Dael, *Liquid Crystals*, **5** (3), 871–875 (1989).
31. D. Armitage, F. P. Price, *J. Appl. Phys.*, **47**, 2735–39 (1976).
32. R. M. Hornreich, S. Shtrikman, *J. Phys. France*, **41**, 335–340 (1980).
33. R. M. Hornreich, S. Shtrikman, *Phys. Lett.*, **82A** (7), 345–9 (1981).
34. R. M. Hornreich, S. Shtrikman, *Mol. Cryst. Liq. Cryst.*, **165**, 183–211 (1988).
35. B. Jérôme, P. Pieranski, *Liquid Crystals*, **5** (3), 799–812 (1989).
36. Basing on spectroscopic and microscopic observations on the compound (+)-2-Methylbutyl-*p*-[(*p*-methoxy-benzylidene)-amino]-cinnamate (MMBC) by W. Kuczyński,^{37,38} an fcc structure was proposed by P. H. Keyes³⁹ for BPII occurring in this material. However, Kossel diagrams described by B. Jérôme *et al.*⁴⁰ reveal a sc structure for BPII for this substance. Comparison between Reference 37 and 40 leads to the conclusion that the first maximum observed in the IR³⁷ was erroneously associated with BPII, but should in fact occur only in BPI.
37. W. Kuczyński, *Mol. Cryst. Liq. Cryst.*, **130**, 1–10 (1985).
38. W. Kuczyński, *Phys. Lett.*, **110 A** (7,8), 405 (1985).
39. P. H. Keyes, *Phys. Rev. Lett.*, **59** (1), 83–85 (1987).
40. B. Jérôme, P. Pieranski, V. Godec, G. Haran, C. Germain, *J. Phys. France*, **49**, 837–844 (1988).
41. S. Meiboom, J. P. Sethna, P. W. Anderson, W. F. Brinkman, *Phys. Rev. Lett.*, **46**, 1216–19 (1981).
42. S. Meiboom, M. Sammon, D. W. Berreman, *Phys. Rev. A*, **28** (6), 3553–60 (1983).
43. J. P. Sethna in: "Theory and Applications of Liquid Crystals," p. 305, edited by J. L. Ericksen and D. Kinderlehrer, Springer, New York (1987).
44. E. Dubois-Violette, B. Pansu, *Mol. Cryst. Liq. Cryst.*, **165**, 151–182 (1988).
45. E. I. Demikov, V. K. Dolganov, S. P. Krylova, *Sov. Phys. JETP Lett.*, **42** (1), 16–19 (1985).
46. E. I. Demikhov, V. K. Dolganov, S. P. Krylova, *Sov. Phys. JETP*, **66** (5), 998–1001 (1987).

47. V. A. Kizel, V. V. Prokhorov, *Sov. Phys. JETP Lett.*, **38** (6), 337–341 (1983).
48. V. A. Kizel, V. V. Prokhorov, *Sov. Phys. JETP*, **60** (2), 257–266 (1984).
49. G. Heppke, H.-S. Kitzerow, M. Krumrey, *Mol. Cryst. Liq. Cryst.*, **150** b, 265–276 (1987).
50. J. H. Flack, P. P. Crooker, R. C. Svoboda, *Phys. Rev. A*, **26** (1), 723 (1982).
51. J. H. Flack, P. P. Crooker, D. L. Johnson, S. Long in: “Liquid Crystals and Ordered Fluids,” Vol. 4, pp. 901–914, Ed.: A. C. Griffen und J. F. Johnson, Plenum Press, New York (1984).
52. J. W. Gorman, P. P. Crooker, *Phys. Rev. A*, **31** (2), 910–13 (1985).
53. R. M. Hornreich, S. Shtrikman, *Phys. Rev. A*, **28** (3), 1791–1807 (1983); Erratum: *Phys. Rev. A*, **28** (6), 3669 (1983).
54. F. Porsch, H. Stegemeyer, *Chem. Phys. Lett.*, **155** (6), 620–623 (1989).
55. P. E. Cladis, T. Garel, P. Pieranski, *Phys. Rev. Lett.*, **57** (22), 2841–44 (1986).
56. W. Kossel, V. Loeck, H. Voges, *Zeitschrift für Physik*, **94**, 139–144 (1935).
57. P. Pieranski, P. E. Cladis, T. Garel, R. Barbet-Massin, *J. Phys. France*, **47**, 139–143 (1986).
58. J. D. H. Donnay, D. Harker, *J. Min. Soc. Am.*, **22**, 446–467 (1937).
59. P. Pieranski, P. E. Cladis, *Liquid Crystals*, **3** (3), 397 (1988).
60. D. Armitage, R. J. Cox, *Mol. Cryst. Liq. Cryst.*, **64** (Lett.), 41–50 (1980).
61. P. L. Finn, P. E. Cladis, *Mol. Cryst. Liq. Cryst.*, **84**, 159–192 (1982).
62. G. Heppke, M. Krumrey, F. Oestreicher, *Mol. Cryst. Liq. Cryst.*, **99**, 99–105 (1983).
63. H. Gleeson, R. Simon, H. J. Coles, *Mol. Cryst. Liq. Cryst.*, **129**, 37–52 (1985).
64. W. H. de Jeu, “Physical Properties of Liquid Crystalline Materials,” Gordon & Breach, New York (1980).
65. H.-S. Kitzerow, Thesis, Technische Universität Berlin 1989.
66. G. Heppke, H.-S. Kitzerow and M. Krumrey, *Mol. Cryst. Liq. Cryst. Lett.*, **1** (3–4), 117 (1985).
67. G. Heppke, B. Jérôme, H.-S. Kitzerow, P. Pieranski, *J. Phys. France*, **50**, 549–562 (1989).
68. G. Heppke, B. Jérôme, H.-S. Kitzerow, P. Pieranski, *J. Phys. France*, **50**, 2991–2998 (1989).
69. B. M. Leon Fong, J. A. Martin-Pereda, *Appl. Opt.*, **24** (17), 2842–45 (1985).
70. J. F. Nye, “Physical Properties of Crystals,” Clarendon Press, Oxford (1957).
71. V. E. Dmitrienko, *Liquid Crystals*, **5** (3), 847–851 (1989).
72. F. Oestreicher, Thesis, Technische Universität Berlin 1984.
73. H. Stegemeyer, F. Porsch, *Phys. Rev. A*, **30** (6), 3369–3371 (1984).
74. D. Lubin, R. M. Hornreich, *Phys. Rev. A*, **36** (2), 849–857 (1987).
75. J. Ziolo, J. Chrapek, S. J. Rzoska, W. Pyzuk, *Mol. Cryst. Liq. Cryst. Lett.*, **3** (6), 183–8 (1986).
76. G. Heppke, H.-S. Kitzerow and M. Krumrey, *Mol. Cryst. Liq. Cryst. Lett.*, **2** (1–2), 59 (1985).
77. F. Porsch, H. Stegemeyer, K. Hiltrop, *Z. Naturforsch.*, **39a**, 475–480 (1984).
78. M. A. Marcus, *Phys. Rev. A*, **25** (4), 2272–2275 (1982).
79. H. Onusseit, H. Stegemeyer, *J. Crystal Growth*, **61**, 409–411 (1983).
80. F. Porsch, H. Stegemeyer, *Liquid Crystals*, **2** (3), 395–9 (1987).
81. G. H. Heilmeyer, L. A. Zanon, *Appl. Phys. Lett.*, **13**, 91 (1968).
82. H. J. Coles, H. F. Gleeson, J. S. Kang, *Liquid Crystals*, **5** (4), 1243–1252 (1989).
83. G. Heppke, H.-S. Kitzerow and F. Oestreicher, unpublished results.
84. F. Porsch, H. Stegemeyer, *Chem. Phys. Lett.*, **125** (4), 319–323 (1986).
85. P. Pieranski, P. E. Cladis, *Chem. Phys. Lett.*, **130** (4), 368–369 (1986).
86. H. Stegemeyer, F. Porsch, K. Hiltrop, *Chem. Phys. Lett.*, **130** (4), 370 (1986).
87. P. Pieranski, P. E. Cladis, R. Barbet-Massin, *J. Phys. Lett.*, **46**, L-973–L-977 (1985).
88. M. Jorand, P. Pieranski, *J. Physique*, **48**, 1197–1205 (1987).
89. F. Porsch, H. Stegemeyer, *Liquid Crystals*, **5** (3), 791–798 (1989).
90. N.-R. Chen, J. T. Ho, *Phys. Rev. A*, **35** (11), 4886–8 (1987).
91. D. K. Yang, P. P. Crooker, *Phys. Rev. A*, **37** (10), 4001–5 (1988).
92. D. K. Yang, P. P. Crooker, *Liquid Crystals*, **7** (3), 411–419 (1990).
93. P. Pieranski, P. E. Cladis, *Phys. Rev. A*, **35** (1), 355–364 (1987).
94. G. Heppke, B. Jérôme, H.-S. Kitzerow, P. Pieranski, *Liquid Crystals*, **5** (3), 813–828 (1989).
95. S. A. Brazovskii, S. G. Dmitriev, *Sov. Phys. JETP*, **42** (3), 497–502 (1976).
96. R. M. Hornreich, M. Kugler, S. Shtrikman, *Phys. Rev. Lett.*, **54** (19), 2099–2102 (1985).
97. R. M. Hornreich, M. Kugler, S. Shtrikman, *J. Phys. Coll.*, **46**, C3-47–C3-60 (1985).
98. R. M. Hornreich, S. Shtrikman, *Liquid Crystals*, **5** (3), 777–789 (1989).
99. R. M. Hornreich, S. Shtrikman, *Phys. Rev. A*, **41** (4), 1978–1989 (1990).
100. G. Heppke, H.-S. Kitzerow, D. Löttsch, Ch. Papenfuß, *Liquid Crystals*, **8** (3), 407–418 (1990).
101. J. G. Kirkwood, I. Oppenheim: “Chemical Thermodynamics,” McGraw-Hill Book Comp., New York (1961).
102. W. Helfrich, *Phys. Rev. Lett.*, **24** (5), 201–3 (1970).
103. C. Motoc, M. Honciuc, *Rev. Rum. Phys.*, **28** (6), 541–6 (1983).
104. H. Stegemeyer, B. Spier, *Chem. Phys. Lett.*, **133** (2), 176–178 (1987).

105. P. Pieranski, P. E. Cladis, R. Barbet-Massin, *J. Phys. France*, **47**, 129–132 (1986).
106. P. Pieranski, P. E. Cladis, R. Barbet-Massin, *Liquid Crystals*, **5** (3), 829–838 (1989).
107. R. M. Hornreich, M. Kugler, S. Shtrikman, *Phys. Rev. Lett.*, **48**, 1404 (1982).
108. P. J. Collings, *Phys. Rev. A*, **30** (4), 1990–93 (1984).
109. V. A. Belyakov, E. I. Demikhov, V. E. Dmitrienko, V. K. Dolganov, *Sov. Phys. JETP*, **62** (6), 1173–82 (1985).
110. V. M. Filev, *Sov. Phys. JETP Lett.*, **43** (11), 677–681 (1986).
111. R. M. Hornreich, S. Shtrikman, *Phys. Rev. Lett.*, **56** (16), 1723–6 (1986).
112. R. M. Hornreich, S. Shtrikman, *Phys. Lett. A*, **115** (9), 451–454 (1986).
113. D. K. Yang, P. P. Crooker, *Liquid Crystals*, **7** (3), 411–419 (1990).
114. H.-S. Kitzerow, P. P. Crooker, S. L. Kwok and G. Heppke, *J. Phys. France*, **51**, 1303–1312 (1990).
115. H.-S. Kitzerow, P. P. Crooker, S. L. Kwok, S. Xu and G. Heppke, *Phys. Rev. A*, **42** (6), 3442–3448 (1990).
116. D. K. Yang, P. P. Crooker, K. Tanimoto, *Phys. Rev. Lett.*, **61** (23), 2685–2688 (1988).
117. V. E. Dmitrienko, private communication.
118. H.-S. Kitzerow, P. P. Crooker and G. Heppke, to be published.
119. P. R. Gerber, *Mol. Cryst. Liq. Cryst.*, **116**, 197–206 (1985).
120. H. J. Coles and H. F. Gleeson, *Liquid Crystals*, **5** (3), 917–926 (1989).
121. H. J. Coles and H. F. Gleeson, *Mol. Cryst. Liq. Cryst.*, **167**, 213–225 (1989).
122. N. A. Clark, S. T. Vohra, M. A. Handschy, *Phys. Rev. Lett.*, **52** (1), 57–60 (1984).
123. W. Helfrich, *Phys. Rev. Lett.*, **23** (7), 372–374 (1990).
124. R. M. Hornreich, private communication.
125. P. G. de Gennes, “The Physics of Liquid Crystals,” Clarendon Press, Oxford (1974).
126. V. M. Filev, *Sov. Phys. JETP Lett.*, **45** (4), 235–238 (1987).
127. R. M. Hornreich, S. Shtrikman, *Phys. Rev. Lett.*, **59** (1), 68–70 (1987).
128. P. G. de Gennes, *Solid State Comm.*, **6**, 163–165 (1968).
129. J. J. Wysocki, J. Adams, W. Haas, *Phys. Rev. Lett.*, **20** (19), 1024–5 (1968).
130. A. I. Feldman, P. P. Crooker, L. M. Goh, *Phys. Rev. A*, **35** (2), 842–845 (1987).